CHAPTER 6
SYSTEM INTEGRATION AND TEST SET-UP: SYNCHRONIZATION AND CONTROL UNITS

This chapter reports lidar system integration in the laboratory and its preliminary tests. First, the chapter begins with a basic outline of the main units that configure the system architecture and the protocol of signals amongst them. Since the receiver unit has already been explained in Chap.4, the chapter progresses to explain the synchronization and control units. Functional operation of the former is highlighted for it takes active part in handshake signals of the system, especially as far as a future mobile system will be concerned. In order to make the text more amenable, the control unit is discussed in a top-level fashion. A more detailed version, which would be useful for system maintenance and troubleshooting can be found referenced among the projects directed (see index). At the end of the chapter, some of the first test set-up experiments conducted are shown in photographs. Since test and measurement of the lidar receiver has already been made in Chap.4 and 5, the tests performed here concentrate on range-calibration of the system through the synchronization unit.

1. LIDAR SYSTEM INTEGRATION

1.1 SYSTEM OVERVIEW

A first introduction to the UPC lidar system was given in Chap.1, Sect.4, where the units that integrate the system were presented. Actual lidar system architecture is based on Fig.1 and on the mirror-based emitting configuration (Chap.1, Sect.4.1). The architecture, however, is designed with a view to guarantee full compatibility between the fixed-station and a future mobile system, discussed in the introduction of this PhD thesis.

Next, let us review the main function of the units that form the architecture of Fig.1.

The unit control is based on a *66-MHz 486 DX* computer and performs these tasks:

1) *GPIB control over all laser parameters* (on/off, lamp energy, pulse-repetition-frequency (PRF), output wavelength, etc).
2) *Data acquisition* via the *20-Msps CompuScope 1012* digitizer. The card is configured to provide *flexible triggering* from either the lidar channel or an external signal. Since the laser fires periodically, the control unit provides a pre-trigger feature so that data acquisition can be triggered from either the control unit or the synchronization unit. Aperture jitter is about *10 ps*.
3) *Estimation of the laser fire jitter from the build-up voltage signal* (Sect.1.2).
4) *Alarm monitoring and supervision.*
5) *User-interface and signalling across the lidar bus* (Sect.1.3).

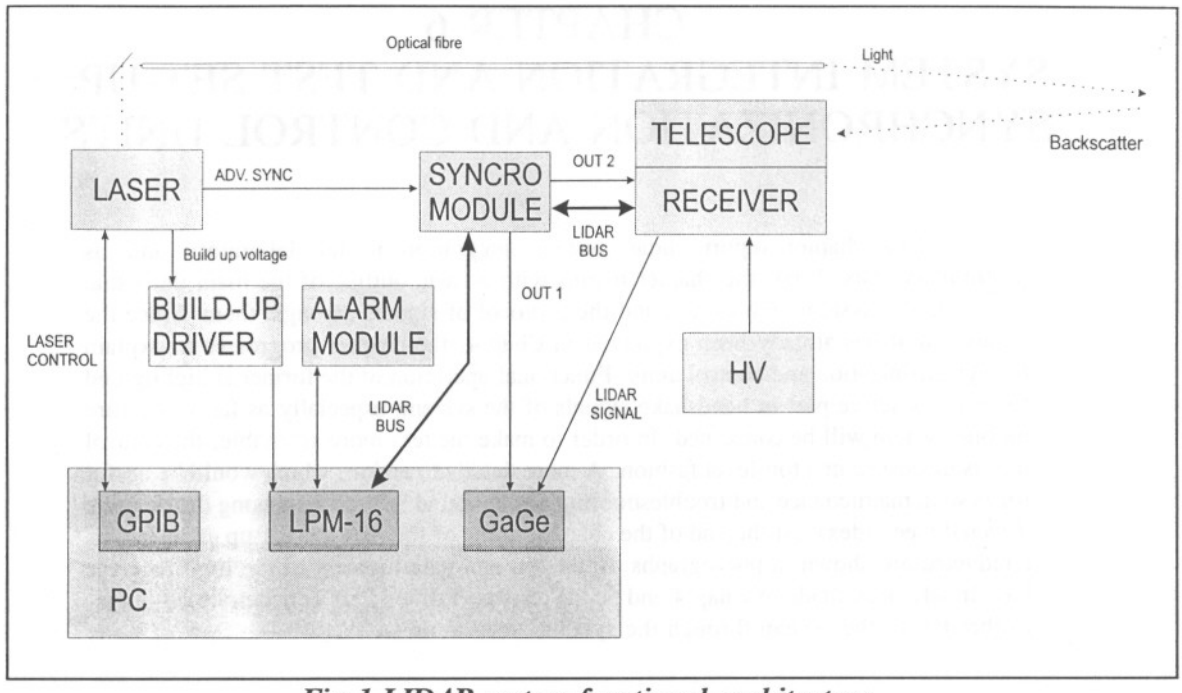

Fig.1 LIDAR system functional architecture.

6) *Real-time preprocessing of lidar raw-data.* This includes adaptive offset cancellation and pulse integration (Sect.3.3.1)

Tasks (3),(4) and (5) use a *PC-LPM-16* multifunction I/O board manufactured by *National Instruments* (Sect.3.2).

As much as the control unit gives instructions to the rest of the equipment, the synchronization unit arbitrates the listen window of the receiver and the acquisition protocol of the system [144]. This can be better understood with regard to the following actions:

1) *Synchronize receiver enable and disable states* to the PRF according to the minimum exploring range (receiver gating). If that range is denoted R_{min}^{s}, the receiver will have to be disabled for a time

$$T_{OUT2} = \frac{2R_{\min}^{s}}{c} + \Delta T_{OUT2} \tag{1}$$

where the first term accounts for the trip-time of the lidar return and the second term is a compensation for system time inaccuracies, mainly, cable delays and jitter (see also Chap.3 Sect.3.3).

2) *Trigger data acquisition* in the control unit (provided pre-trigger mode in the control unit is not used). Acquisition will have to be triggered at

$$T_{OUT1} = \frac{2R_{\min}^{s}}{c} + \Delta T_{OUT1} \tag{2}$$

Note that corrections $\Delta T_1, \Delta T_2$ are different.

3) *Arbitrate requests from the control unit to change receiver and range parameters.*

4) *Update new gains and offsets in the receiver.*

Tasks (3) and (4) are performed in conjunction with the digital receiver mentioned in the introduction since if the the analog receiver is to be used, gain and offset parameters will have to be changed manually.

Note that in the minimum configuration of the lidar system, that is, when the system works with the analog receiver and acquisition is pre-triggered from the acquisition card itself, the synchronization unit can be made redundant. The need of a synchronization unit arises in the mobile system when interspersed scans having different minimum ranges and gains are wished. The control unit is not fast enough to change exploring parameters and to carry out acquisition and raw-data preprocessing within the same *pulse-repetition-time (PRT)*. System parameters would include *minimum exploring range of the system, gain and receiver offset*. These parameters ought to be changed out of the listen window, otherwise lidar-return information can be destroyed.

Fig.2 shows the control room along with the laser. By means of a mirror, the laser beam is output vertically to the dome, which is placed above the control room. A tube is used to communicate the room with the dome and to prevent accidents with the laser beam.

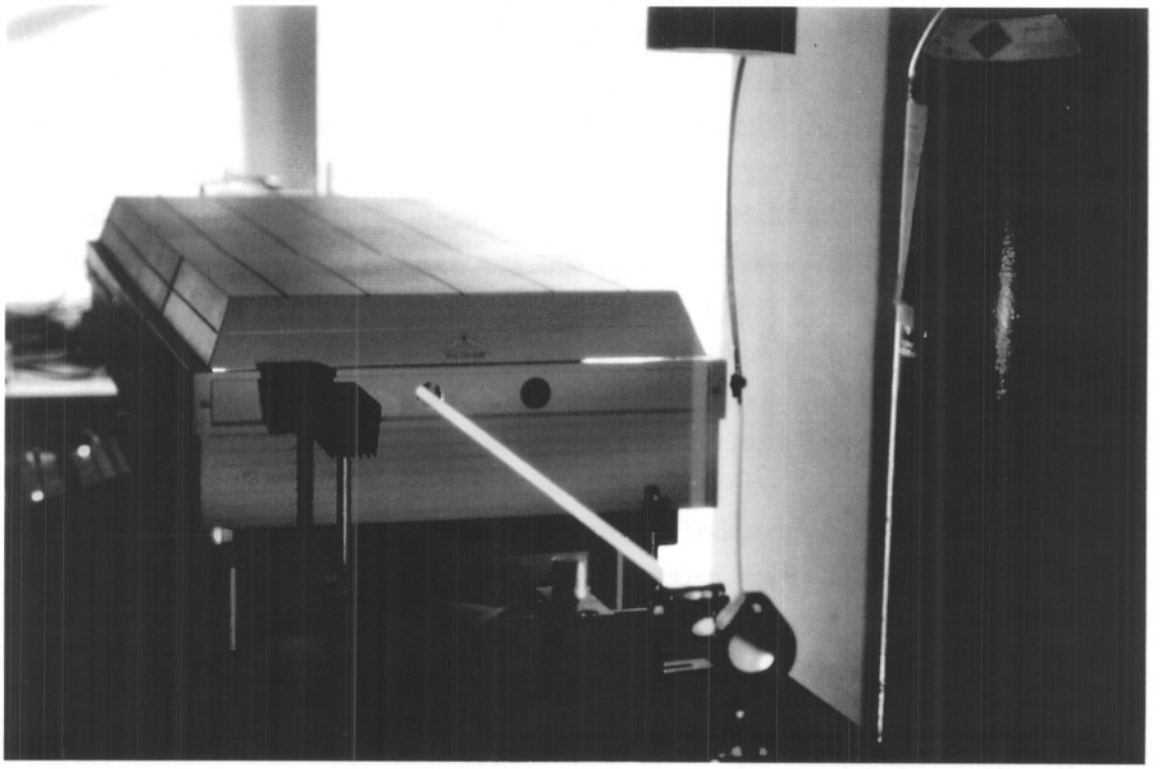

Fig.2 Actual configuration of the lidar system.

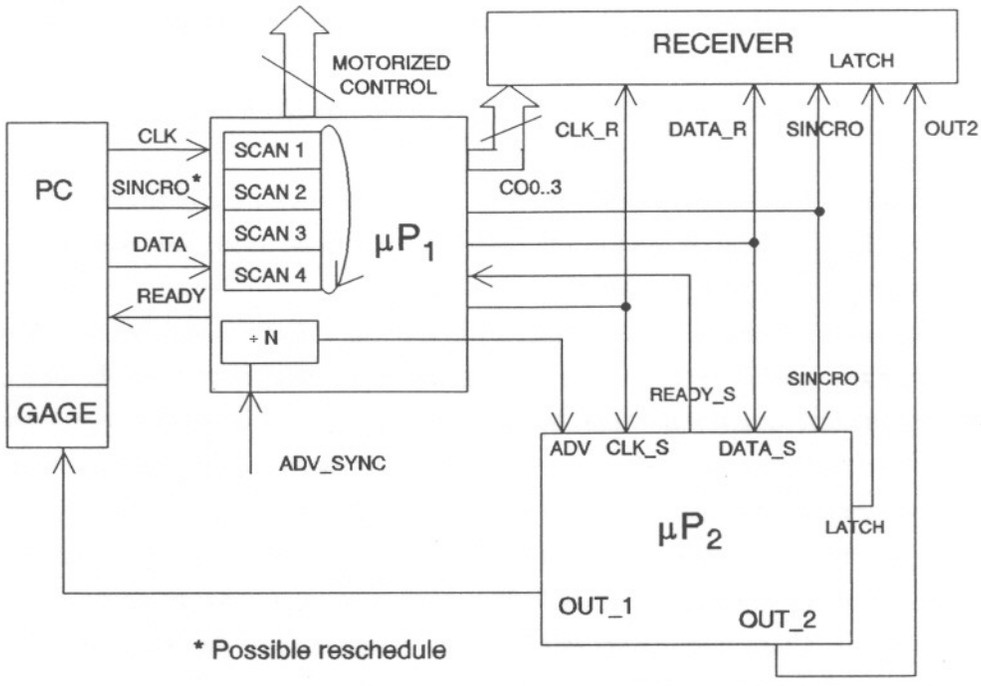

Fig.3 Planned synchronization and trunking μP-units for the mobile system.

Fig.3 depicts a block diagram schematic of the planned protocol configuration for the mobile system. Signal protocol will be carried out by two microprocessors, μP_1 and μP_2. μP_1 receives data words from the control unit indicating scan parameters (e.g. minimum scan range, receiver gain, receiver offset correction, etc.) and scan area coordinates (elevation, azimuth and incremental steps). For each fire coordinate, the microprocessor starts a round-robin sequence where scan parameters are changed. In the example of Fig.3, the microprocessor would begin with *scan_word_1* and end with scan_word_4. This first microprocessor acts as a trunking node. Thus, for instance, once information from *scan_word_1* had been demultiplexed, gain and offset data would be output to the receiver via ports CO_0-CO_3 and *DATA_R,* and time delay data (delay word) corresponding to the preset minimum range would be passed to μP_2. μP_2 is a timing microprocessor and it corresponds to the synchronization unit described in Sect.2 of this chapter (either as a buffered synchronization unit or as a microprocessor-based unit). μP_2 is synchronized by the *Advanced Synchronism Master Clock* of the laser, so that the laser fire time is known. Once μP_2 receives the delay word from μP_1, it stores the word and it basically waits for the next laser fire. At the next fire, the new minimum exploring range is updated, a syncronization burst is sent to the receiver via the *LATCH* line to force gain and offset parameters to update and a time delay count corresponding to that exploring range begins (eqs.(1) and (2)). Once timeout occurs, the receiver is enabled via the OUT_2 line and a new listen window begins for the receiver; data acquisition is triggered via the

OUT1 and a *READY_S* request to send a new *scan word* at the next PRF is put to μP_1.

If the control unit is too burdened with data acquisition, one out of two or even two out of three laser shots may be lost. In fact, this is actually the case of our system. This is equivalent to say, that the effective PRF is reduced by a factor 2 or 3. To accommodate this parameter, the diagram of Fig.3 includes a frequency preescaler by N that is connected at the output of the *Advanced Synchronism Master Clock.*

From what has been explained, it is clear that the function of μP_1 is to guarantee synchronous enable of the receiver and to trigger data acquistion at $R_{min}{}^{s}$ within the PRT. As a result, if the lidar is to scan the same range forever and the acquistion card is set to pre-trigger mode (i.e. triggered by the laser Master Clock), *the synchronization unit is made redundant.* The receiver can be left permanently enabled and saturated data can be discarded.

1.2 Laser synchronization signals

1.2.1 Advanced synchronism

Once population inversion has built up in the Nd:YAG rod, the internal trigger source opens the *Q-switch* [26][33]. To perform this action a high voltage output of the Marx bank changes the polarization characteristic of the Pockels cell crystal [36]. At the same time, the Mark bank (Pockels cell driver) is triggered, the timing system outputs a sync signal at the BNC *Q-switch Sync Output.* The *Q-switch Adv Sync Output* is also derived from the internal trigger source of the laser and it can either precede or follow the opening of the Q-switch or equivalently, the *Q-switch Sync Output.* This pre- or post-trigger pulse can be programmed via GPIB from the control unit with ± 500 *ns* [118].

In the lidar system, the *Q-switch Adv Sync Output* is adjusted to its maximum pre-trigger value, so that it provides an effective sync signal before the laser light output. *In Fig.1 this signal informs the sync unit that a laser shot is about to be fired.* Experimentation has shown that laser delays cause the light output to appear later than the *500 ns* expected. The effective time of laser light output is a function of the pulse energy but can be made readily stable by calibrating the system for each laser output. In the control unit, this calibration has been performed only for the maximum energy. In addition long time dithers that can be removed using a *build-up correction* (see next section). In Sect.2.3.3 simple mathematical models combine these two signals to provide fairly stable synchronism.

Very often, lasers are not so sophisticated and they do not provide an Adv Sync output. In such instances a zero-time marker (e.g. using an optical fibre coupled to the light outlet) is used [25]. The main disadvantage of this system is that very fast electronics are needed to prevent that electronic delays seriously limit synchronization of the minimum exploring range of the system (eq.(1)). Verly low thermal-drift is also of concern.

1.2.2 Build-up correction

The Nd:YAG laser described in Chap.1 can be operated in seeded and unseeded modes. During seeded operation, very narrow linewidth *($\Delta\upsilon < 10$ kHz)* laser emission of *> 4 mW* is directed on-axis into the host laser cavity.

The time during which the spontaneous noise emission is up to the saturation fluence level (the level where a pulse can begin to be observed being emitted from the host laser) is termed the *Q-switch* pulse build-up time.

When the host laser is seeded, there is approximately a *15-ns* reduction in Q-switch build-up time. Under these circumstances, there will be at least *1000* times more energy in the seeded longitudinal mode frequency that in any other longitudinal mode and consequently, pulse spectral characteristics are greatly enhanced.

Since the seed laser and host cavities are independent entities some frequency control and stabilization are required. Frequency stabilization is achieved via active control of the host cavity length. The high reflecting mirror of the host resonator is mechanically translated by a piezoelectric *frequency tuning element (FTE),* which allows for fast correction in the frequency of the host. Fig.4 suggests that minimizing the Q-switch build-up time corresponds to proper injection seeding. Consequently, this is the parameter employed to properly translate the piezoelectric FTE for precise frequency overlap [116].

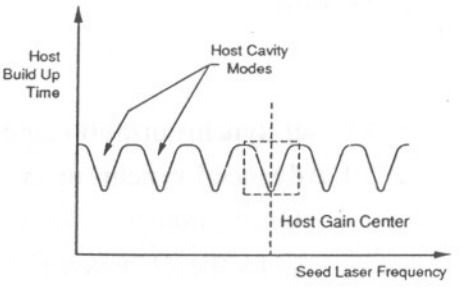

Fig.4 Host laser build-up time versus seed laser frequency [116].

The control loop block diagram for build-up time minimization is shown in Fig.5. To minimize the *Q-switch* build-up time, the control electronics develop an error signal using the derivative of the build-up time with respect to the host cavity length *(dT_b/dl)*. This is essentially the slope of the curves in Fig.4.

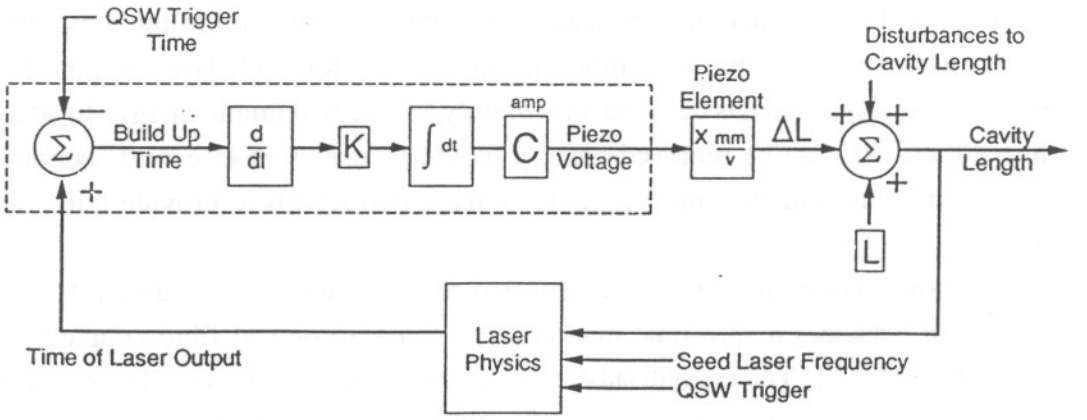

Fig.5 Frequency control loop-block diagram [116].

When this error signal is zero, the *Q-switch* build-up time is at its minimum value for that host cavity length. The error signal is integrated over time to produce the piezoelectric FT control voltage. Because the control loop uses integral control an average steady state error value of zero is possible and thereby optimum frequency overlap between the seed laser and the host laser is achieved.

The laser has a BNC output that is correlated with *Q-switch* build-up time and that ranges from *8 V* (long build-up time) to *0 V* (instantaneous build-up time) [116]. The relationship between build-up voltage, V_b, and *Q-switch* build-up time, T_b, is *0.05 V/ns*,

$$T_b = \frac{V_b}{0.05} \qquad [ns] \tag{3}$$

Measurements have shown that the build-up voltage output is even active in unseeded operation. *In this mode, the build-up time is not minimized but still carries information on time prediction of laser output.* From the diagram of Fig.5, the build up time represents the prediction error between the estimated and actual time of laser output, and consequently it is an useful adaptive correction to the time information provided by the *Advanced Sync Output*.

1.3 Signal protocol

1.3.1 The lidar bus

The lidar bus is formed by eight lines, one of which has multiplexed functions. The lidar bus starts in the control unit (the PC) and links the sync and receiver units to the PC. It conveys information on different parameters concerning the minimum sync lidar range, $R_{min}{}^{s}$ such as range, scale, timer data and information concerning the digital lidar receiver such as gain and offset parameters. See also Tab.1.

Data format in the DQ_1 line depends on the listener unit. If data is for the sync unit, a 40-bit word format is followed (Fig.7). The bit *REC* selects the receiver mode (synchronized or permanently disabled), the bit *SCALE* selects the range scale (low range-high resolution, normal range-normal resolution) and the remaining 34 bits, convey information to program internal timing potentiometers of the unit. If data is for the receiver unit, the word length depends on the receiver function encoded by lines CO_0-CO_3. Thus, for instance, gain is programmed by one 6-bit word and offset is programmed by one 16-bit word (digital-to-analog conversion). For other functions refer to the receiver's manual.

1.3.2 Other protocol signals

The sync unit issues two protocol signals named OUT_1 and OUT_2. These signals do not belong to the lidar bus but they are coaxial lines that are connected to the acquisition card trigger and to the receiver enable, respectively.

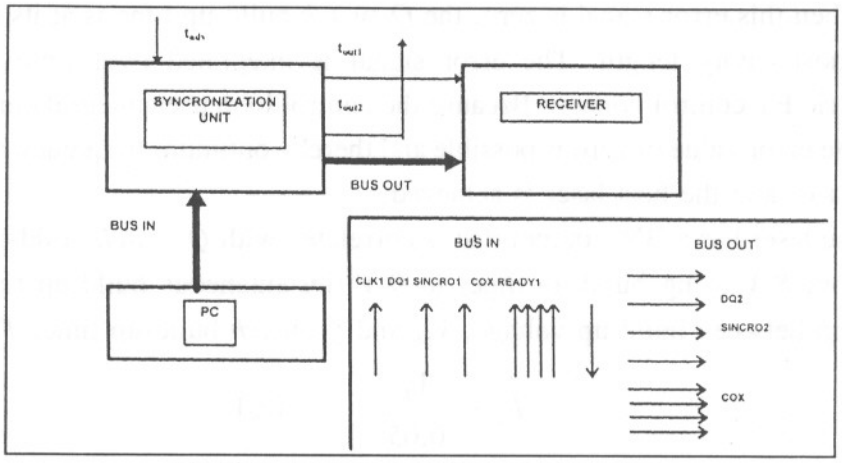

Fig.6 Lidar bus and line specification.

The fact that the sync unit uses two different signals instead of only one is justified from the physical arrangement of the lidar set-up of Fig.1 and the line delays associated. The control room and the telescope are separated *9 m*, which represent a *47-ns* delay.

LINE DESIGNATIONS & DESCRIPTIONS

Non multiplexed lines	(7 lines)
CO_0-CO_3	Parallel data from the control unit used to encode receiver operation modes.
$SINCRO_1$	Select signal from the control unit indicating that bus data is for the sync unit (1) or for the receiver unit (0).
DQ_1	Serial data from the control unit carrying data bursts to the sync and receiver units.
CLK_1	Clock line from the control unit that determines data transfer rates.
Multiplexed lines	(1 line)
$READY_1$	Flag signal from the sync unit to the control unit indicating that access is granted to the control unit.
LATCH	Serial line from the sync unit that carries a 4-bit burst that triggers gain and offset updates in the receiver.

Tab.1 Lidar bus line designations & descriptions.

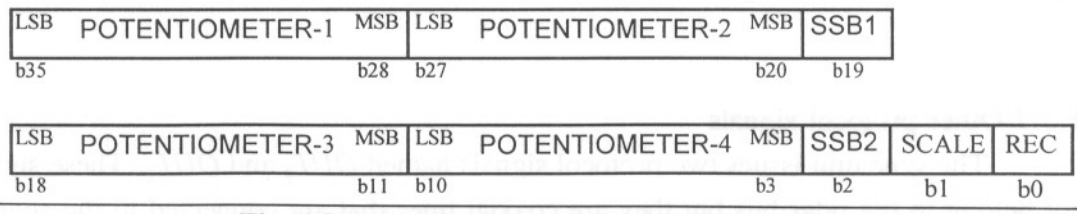

Fig.7 Synchronization unit 40-bit data word.

Line delays are compensated so that the trigger signal is about a few samples ahead of the enable signal. In this manner, the lidar signal recorded includes the receiver enable transition for verification purposes.

In addition, logic levels and interpretation of the two lines are different. As much as the acquisition card trigger is TTL compatible and it occurs at a LOW-to-HIGH transition of the trigger signal, the receiver enable is an *open colector* signal. Enable and disable voltage thresholds were given in Tab.5 Chap.4. These signals will be explained later in more detail in Sect.2.2.

Other protocol signals include the *Advanced Sync Signal,*, which is the master synchronization signal of the system, and the *Build-Up Correction Signal.* Both have been described in Sect.1.2. As for the latter, an AD converter in the PC-LPM-16 interface card of the control unit samples this signal to have an estimation of the *Advanced Sync Signal* drift. (The build-up driver of Fig.1 is basically used for signal conditioning). The sync control icon in the control program provides a feature that allows adaptive correction of the delay time. This will be discussed in Sect.3.

Both the laser and the high voltage supply (which is denoted *HV* in the block diagram of Fig.1) can be controlled via GPIB from the control unit but now only the former is controlled.

Finally, as far as the alarm module is concerned, this module is still in development and it is to be connected to the PC-LPM-16 interface card to the control units and its main application will be for the mobile system. For the time being, a remote interlock fault switch, which is controlled by a person in the building roof, is included in the interlock chain. The laser shuts off if the switch fails to be pressed.

2. THE SYNCHRONIZATION UNIT

2.1 Specification overview

In Sect.1.1, the sync unit tasks have been clearly defined. Next, sync specs from Chap.3 Sect.3.3 are reproduced below in Tab.2 in form of minimum rage, $R_{min}{}^{s}$ and *trip-time delays:*

$R_{min}{}^{s}$ = 100 m (0.66 μs)	$R_{max}{}^{s}$ = 2 km (13.3 μs)

Tab.2 Synchronization unit specs.

2.2 Functional diagram and operation

The functional diagram of the sync unit can be better understood by reference to the time waveforms of Fig.8, the mnemonics of Tab.3, the propagation line delays indicated in Fig.25 and the functional diagram of Fig.9.

In Fig.8, it is shown how the time operation of the sync unit is controlled by the *Advanced Sync Output* of the laser. The rising edge of this signal triggers T_1-*ns* timer of the unit. When timeout occurs, the receiver is enabled for *1-ms* time gate. This is equivalent to a listen window of *150 km,* which is more than enough for any lidar-return signal. In order to synchronize the acquisition trigger to the listen window (receiver enable), timer T_2, which is cascaded to timer T_1, offsets delay unbalances between OUT_1 and OUT_2 branches. According to Fig.8, if T_{OUT1} is the effective delay of branch *OUT1*

$$T_{OUT2} = T_1' + \Delta_2' + t_{enable} \tag{4}$$

and T_{OUT2} is the effective delay of branch OUT_2

$$T_{OUT1} = T_1' + T_2' + \Delta_1 \tag{5}$$

synchronous acquisition to the beginning of the listen window is achieved when both effective delays are equal. Mathematically,

$$T_2' \leq \Delta_2' - \Delta_1 + t_{enable} \tag{6}$$

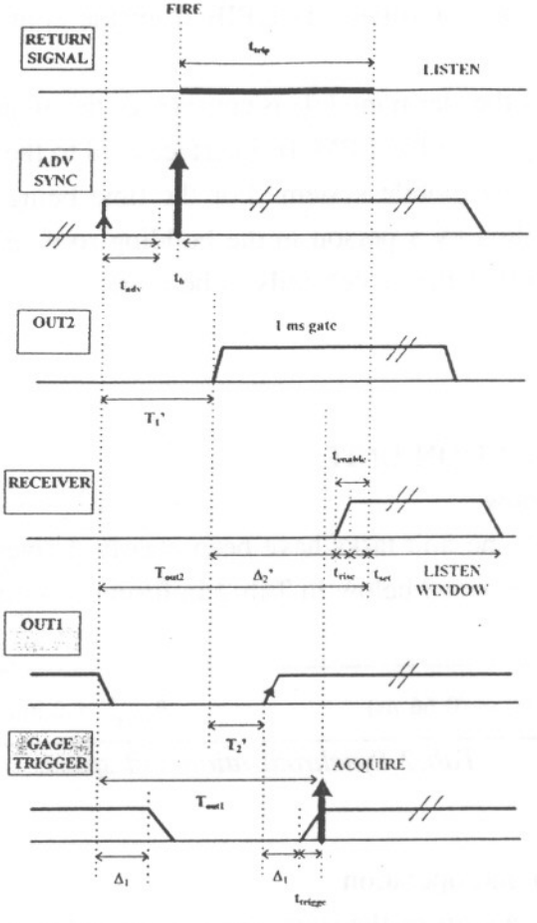

Fig.8 Sync unit time waveforms.

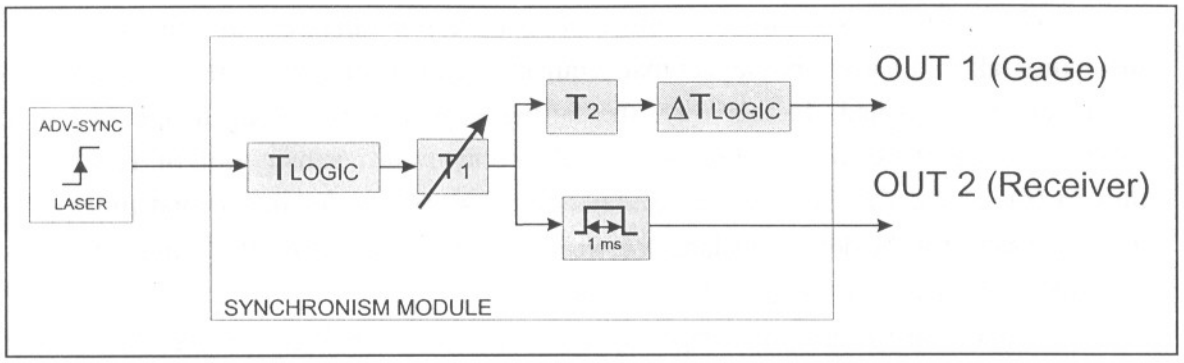

Fig.9 Sync unit functional diagram.

TIME DESIGNATIONS & DESCRIPTIONS

(values show actual performance)

MNEMONIC AND FUNCTION		VALUE
t_{trip}	*Trip time* Is the go-and-return time defined at the minimum range, $R_{min}{}^{s}$. See specs. in Tab.2.	
t_{adv}	*Advanced Sync Time* Fire warning signal to be programmed between *700 ns* and *1 μs*.	700 ns
T_b	*Build-up Time* This time can be interpreted as the prediction error in the estimation of t_{adv}. If enabled by the control unit, it can be used as a correction of the Advanced Sync Time.	
T_1'	*Master timer delay* Is the master timer delay of the sync unit including intrinsic logic delays. From Fig.9, it can be expressed as $T_{logic}+T_1$.	T_1+64 ns
T_2'	*Secondary timer delay* It is the secondary delay of the sync unit including intrinsic logic delays. From Fig.9, it can be expressed as $\Delta T_{logic}+T_2$ (OUT_1 branch).	T_2+20 ns
Δ_1	*Gage trigger line delay* It accounts for the C_OUT_1 line delay indicated in Fig.25.	144 ns
Δ_2'	*Receiver line delay* It accounts for the sum of C_OUT_2 and C_OUT line delays indicated in Fig.25. Since trigger and acquisition synchronization is achieved in the digitizer, this parameter includes the line C_OUT delay.	47+174 ns
T_{OUT1}	*OUT_1 effective delay* This parameter represents the effective time delay between the Adv Sync rising edge and the time when acquisition is triggered.	
T_{OUT2}	*OUT_2 effective delay* This parameter represents the effective time delay between the Adv Sync rising edge and the time when the receiver listen window begins. This accommodates rise and settle times of the receiver.	
t_{on}	*Receiver listen window.* During this time the receiver is enabled and it listens for a lidar-return.	1 ms
t_{enable}	*Receiver enable time.* This time includes both the rise time (10%-90%) (OFF to ON state), which equals *380 ns*, and the 10-% settling time of the receiver.	750 ns

Tab.3 Time waveform parameters, description and measured values.

This relation is defined as the *time calibration equation* of the system. The inequality takes into account the fact that acquisition can be triggered a few samples before the receiver is enabled. In this way, the falling edge corresponding to the end of the receiver disable window can be recorded in the control unit. Substitution of Tab.3 values into eq.(6) yields, $T_2' = 827\ ns$ or equivalently, $T_2 = 807\ ns$ for the second timer. Since it compensates for the delay unbalance between branches OUT_1 and OUT_2, this timer needs be calibrated only once for each lidar set-up.

In addition to these time signals, it was discussed in Sect.1.1 that the sync unit should arbitrate requests from the control unit in order to change receiver and range parameters. That would be the case of programmation of a new minimum exploration range. Since this would mean setting a new delay to timer T_1, this reprogrammation cannot be made at random during the pulse-repetition period *(PRP)*. On the contrary, the sync unit must wait for the end of the receiver *listen window* (about $T_3 = 1\ ms$ later than the *Advanced Sync Master Trigger*) and then update the timer. In practice, this arbitration is accomplished by means of a fourth timer that allows *90-ms* access to the *master sync unit* (the *timer unit*) and a buffer stage that, as its name suggest, buffers data from the control unit. This design leaves about *9-ms* guard time to the beginning of the new PRT, whose duration is *100 ms (PRF= 10 Hz)*. The internal structure of the sync unit, including the buffer and the master unit (timing unit) is shown in Fig.10.

The need for a buffer module can be further justified because of the low transfer rate of the PC-LPM-16 interface card. Speed basically depends on the control load over the control unit. Interface communications are low priority tasks and consequently, they suffer interruptions from high priority tasks (e.g. DMA acquisition, display and real time pre-processing) very often. Measurement of the CLK_1 line frequency confirmed such behaviour. Were not for the buffer, it would be impossible for the sync unit to send the entire *40-bit word* (which conveys the new minimum range) within the access time *(90 ms or less)*. By buffering and appropriate handshake, the sync unit allows dual operation: *asynchronous low speed data transfer from the control unit and synchronous (i.e. outside the listen window) fast speed data transfer to the master sync unit (timer unit).*

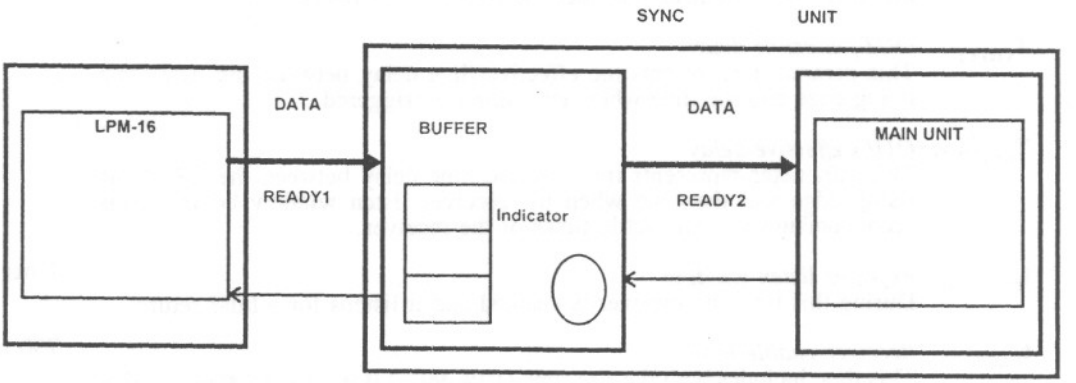

Fig.10 Functional structure of the sync unit and control unit interface.

2.3 Buffered synchronization unit

The sync unit is formed by the two modules shown in Fig.11. The first one is the *buffer module*. It is based on shift-registers and reads the 40-bit word data from the control unit. The second module is the *master sync* module or *timing module*. For clarity reasons, these modules will be explained separately in the following subsections. Let us begin by the timing module and its design equations.

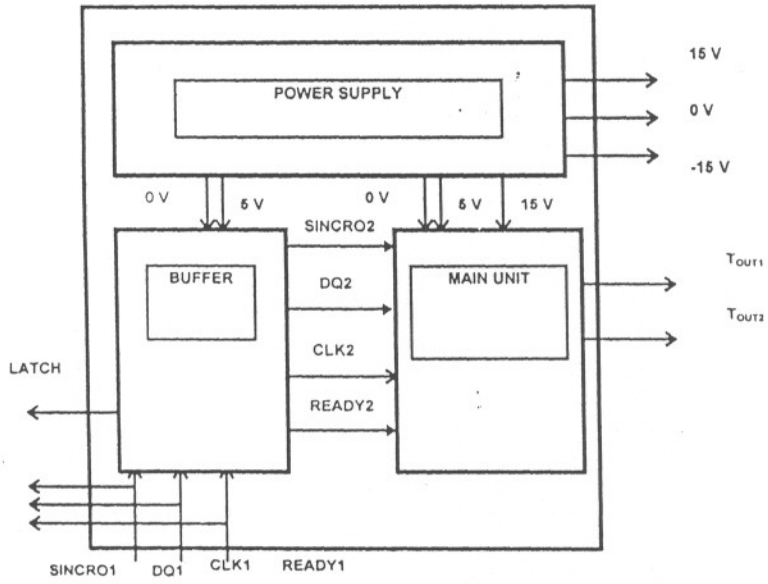

Fig.11 Diagram block of the synchronization unit.

2.3.1 Timing module

The timing module contains the three timers already described in Fig.9 (T_1, T_2 and *1-ms* gate), which are responsible for the time waveforms of Fig.8, and the timer T_4 that controls the access time to perform a rewrite operation in the digital potentiometers (new T_1). The timers are based on four *DS1867* digital timing resistors, *74121* monostable multivibrators and one *74HC4053* multiplexer.

The *DS1867* is a nonvolatile dual digital potentiometer manufactured by Dallas Semiconductor. It consists of two digitally controlled potentiometers having *256-position* wiper settings. Wiper position is maintained in the absence of power through the use of an internal EEPROM memory. Communication and control of the device is accomplished over a 3-wire serial port which allows reads and writes of the wiper position.

The *74121* is a monostable multivibrator with Schmitt trigger input which is virtually immune to temperature and voltage variations. Pulse stability is only limited by the accuracy of the external R_{ext}-C_{ext} net. Throughout the capacity range *(10 pF to 10 μF)* and resistance range *(2 kΩ to 40 kΩ)*, pulse width is defined by the well-known relationship

$$t_w = R_{ext} C_{ext} \ln 2 \tag{7}$$

With reference to Fig.9, the timer blocks denoted T_1, T_2 and *1-ms gate* are clearly indicated in Fig.12. The fourth timer, T_4, provides the line denoted *READY* in Fig.12.

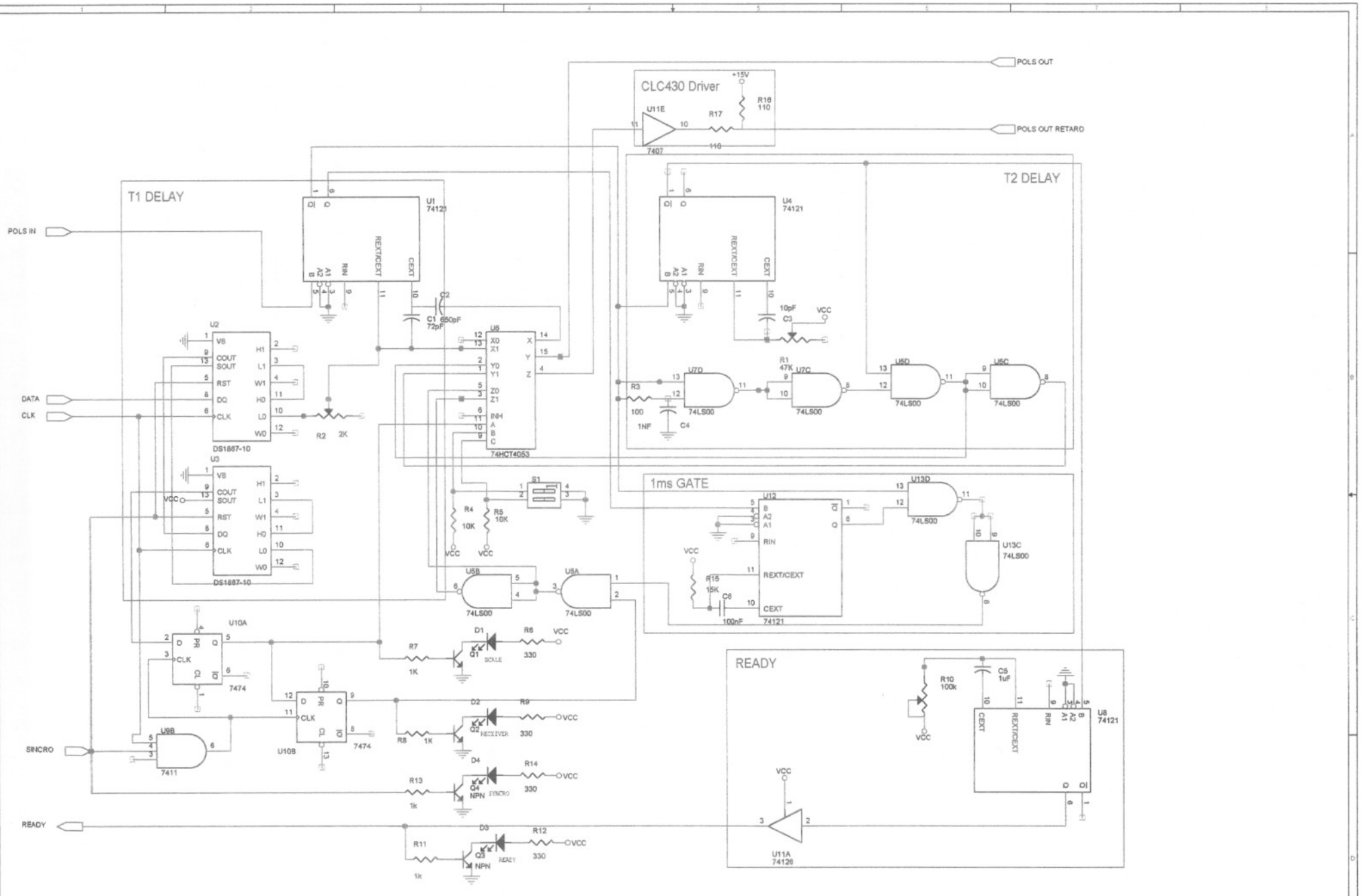

Synchronization unit		
Size A3	Document Number Fig. 12 Sync unit timer circuit	Rev 2
Date: Friday, August 16, 1996	Sheet 1 of 1	

In the design of timer T_1, four digital potentiometers based on two *DS1867-010* units are stacked for increased total resistance *(40 kΩ)* with the same resolution. Capacity multiplexation using one *74HC4053* multiplexer enables to change the timer scale. This allows two different resolution ranges. Since other timers of the unit are not programmable and accuracy is not critic, time delays are adjusted by means conventional trimming resistors.

In the circuit design of Fig.12, two flip-flops are cascaded to the stack of digital potentiometers. They load the *REC* and *SCALE* bits of Fig.7. The first bit (*b0* in the 40-bit data word of Fig.7) conveys information on the receiver disable mode. If this bit is set, the receiver is controlled by the timer unit in the way explained (see time waveforms of Fig.8); otherwise, the receiver is disabled during the whole PRT. The second bit (*b1* of the 40-bit data word of Fig.7) changes the range scale by activating the multiplexer.

Now that the functional blocks of Fig.9 have been implemented in the design of Fig.12 let us derive the basic time-range relationships of the system.

The minimum system range, $R_{min}^{\ s}$ is determined by the time delay of the timer T_1. If the calibration condition of eq.(6) is met, the range where the receiver window begins can indistinctly be computed from the effective time delay, T_{OUT1} or T_{OUT2} in the following manner:

$$R_{\min}^{s} = \frac{c}{2}[T_{OUT1}(T_1) - t_{adv} - T_b] \tag{8}$$

where:

c is the speed of light,
T_1 is the digital time delay set in timer T_1 and,
the rest of variables have already been defined in Tab.3.

Equivalently, if eq.(4) is substituted into eq.(8) above, it yields

$$R_{\min}^{s} = \frac{c}{2}(R_{ext}C_{ext}\ln 2 + T_{logic} + \Delta_2' + t_{enable} - t_{adv} - T_b) \tag{9}$$

where:

R_{ext} is the external timing resistance of the DS1867-010 digital potentiometers,
C_{ext} is the external capacitance multiplexed at the C_{ext} input of the 74121 timer and,
the rest of variables have already been defined in Tab.3.

In the design of Fig.12, R_2 adjusts the minimum R_{ext} to *2 kΩ*, which includes the wiper resistance of the DS1867-010.

Range resolution is defined as the $R_{min}^{\ s}$ range increment for 1 LSB change (i.e *10kΩ/256*) in the master timer T_1. If the time increment is denoted ΔT, then

$$\Delta T = \Delta R_{ext}C_{ext}\ln 2 \rightarrow \qquad \Delta R = \frac{c}{2}\Delta T \tag{10}$$

Tab.4 gives numerical values for the unit designed assuming $T_b=0$. In practice, resolution is ultimately limited by amount of Adv Sync jitter that is left uncorrected.

MASTER SYNC UNIT DESIGN

Precision low-range scale			
Timing net:	C_{ext} = 72 pF	$R_{ext} \epsilon$ (2 kΩ, 40 kΩ)	DS1867-010
Resolution (eq.(10)):	ΔT = 2 ns		ΔR = 0.3 m*
Minimum R_{min}^{s} (eq.(9)):	T_1 = 100 ns	T_{OUT1} = 1135 ns	R_{min1}^{s} = 65.3 m
Maximum R_{min}^{s} (eq.(9)):	T_1 = 1.996 μs	T_{OUT1} = 3.031 μs	R_{min2}^{s} = 349.7 m
Normal range scale			
Timing net:	C_{ext} = 720 pF	$R_{ext} \epsilon$ (2 kΩ, 40 kΩ)	DS1867-010
Resolution (eq.(10)):	ΔT = 20 ns		ΔR = 3 m*
Minimum R_{min}^{s} (eq.(9)):	T_1 = 1 μs	T_{OUT1} = 2.03 μs	R_{min1}^{s} = 200 m
Maximum R_{min}^{s} (eq.(9)):	T_1 = 19.96 μs	T_{OUT1} = 21.00 μs	R_{min2}^{s} = 3150 m
Build-up correction:	$\Delta T = \pm$ 20 ns/V (eq.(3))		$\Delta R = \pm$ 3 m/V

(*) Range resolution calculations assume $T_b = 0$.

Tab.4 Synchronization unit time-range expected performance.

LINE DESIGNATIONS & DESCRIPTIONS

Module-to-module handshake (4 lines)

CLK_2	Clock frequency to empty the buffer (300 kHz). This clock is internally generated by the buffer and it is independent from that of the control unit.
DQ_2	Serial data line from the buffer to the timing unit. It outputs the first 36 bits of the *40-bit* word buffered. These bits are used to rewrite the four digital potentiometers and the scale and receiver disable mode flip-flops.
$READY_2$	This signal is output by the timer unit every PRT to indicate that access to the timer unit is granted. READY timer determines the access window interval, which is currently set to *90 ms*.
$SINCRO_2$	Data input enable to the timer unit that services a buffer request to empty.

External handshake (2 lines)

$READY_1$	Flag signal from the buffer to the control unit indicating that the buffer is empty and available to the control unit.
LATCH	Serial line from the sync unit that carries a 4-bit burst to the receiver. When the buffer empties its *40-bit* word to the timing unit, the 4-bit burst is demultiplexed from the word's tail and passed to the receiver to force gain and offset updates.

Bypassed lines (7 lines) See Tab.1.

$SINCRO_1$,DQ_1,CLK_1	Lidar bus lines used by the sync unit and the digital receiver.
CO_0-CO_3	Lidar bus lines only used by the digital receiver. (Not shown in Fig.11)

Tab.5 Synchronization unit handshake lines.

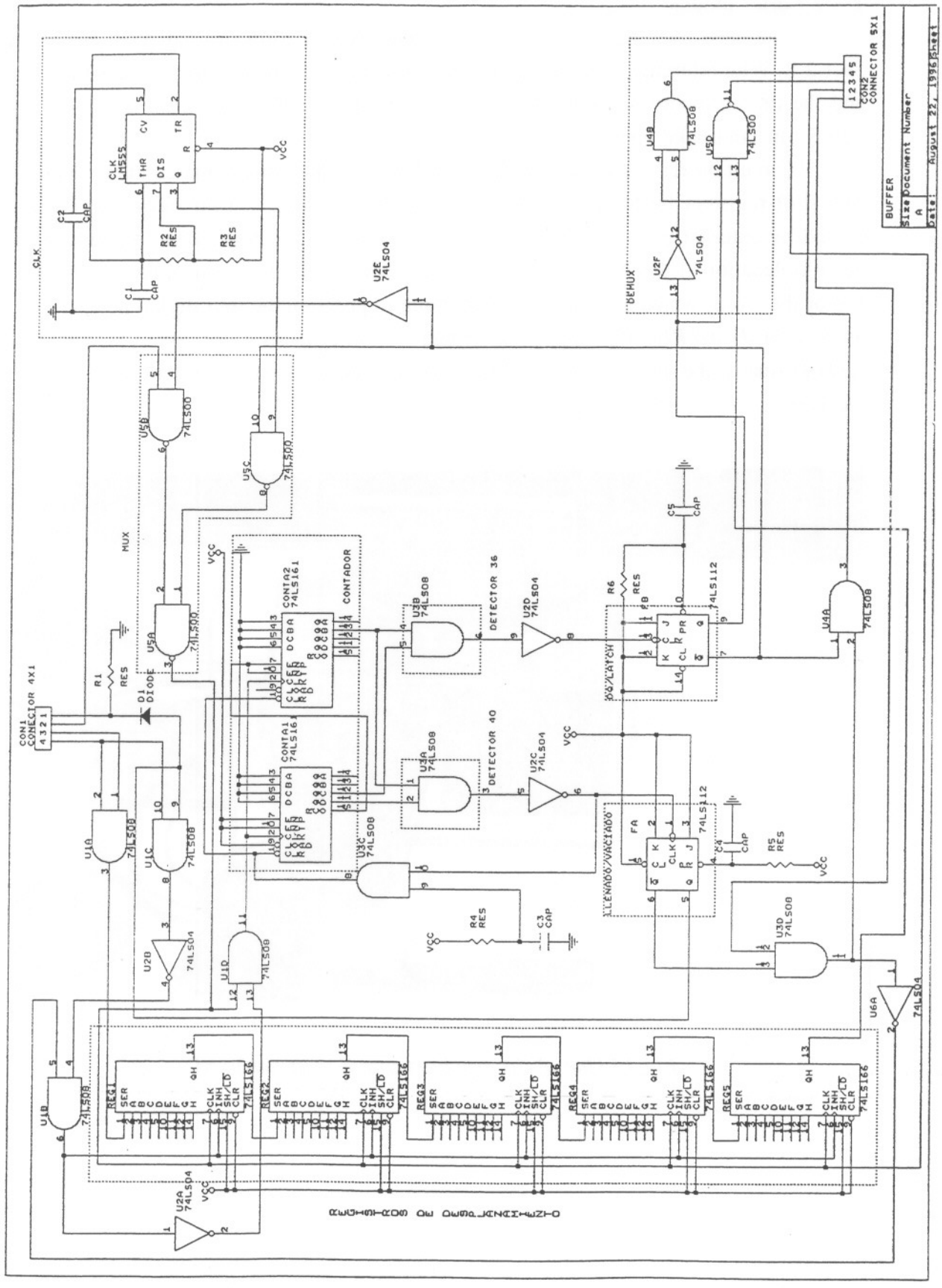

Fig.13 Sync unit buffer circuit.

2.3.2 Buffer module

The need for a buffer module (either hardware or software) has been justified in Sect.2.2. With reference to the functional diagram of Fig.11, handshake between the buffer and the timing modules is done via $SINCRO_2$, $READY_2$, CLK_2 *and* DQ_2 lines. Refer to Tab.5 for handshake operation.

Circuit buffer design is reproduced in Fig.13, where functional circuits are boxed. The shift-registers buffer the *40-bit* word structure of Fig.7. Two binary up-counters helped by external gating are used as 36- and 40-count detectors. These signals control demultiplexation of the 40-bit words in two sections. The first section contains the first *36 bits* or the word, which are sent to the timer unit to program the four digital potentiometer units, *SCALE* and *REC* flip-flops. The second section contains *4 bits,* and it is sent by the *LATCH* line to the digital receiver. This *LATCH* signal is a synchronization burst to the receiver.

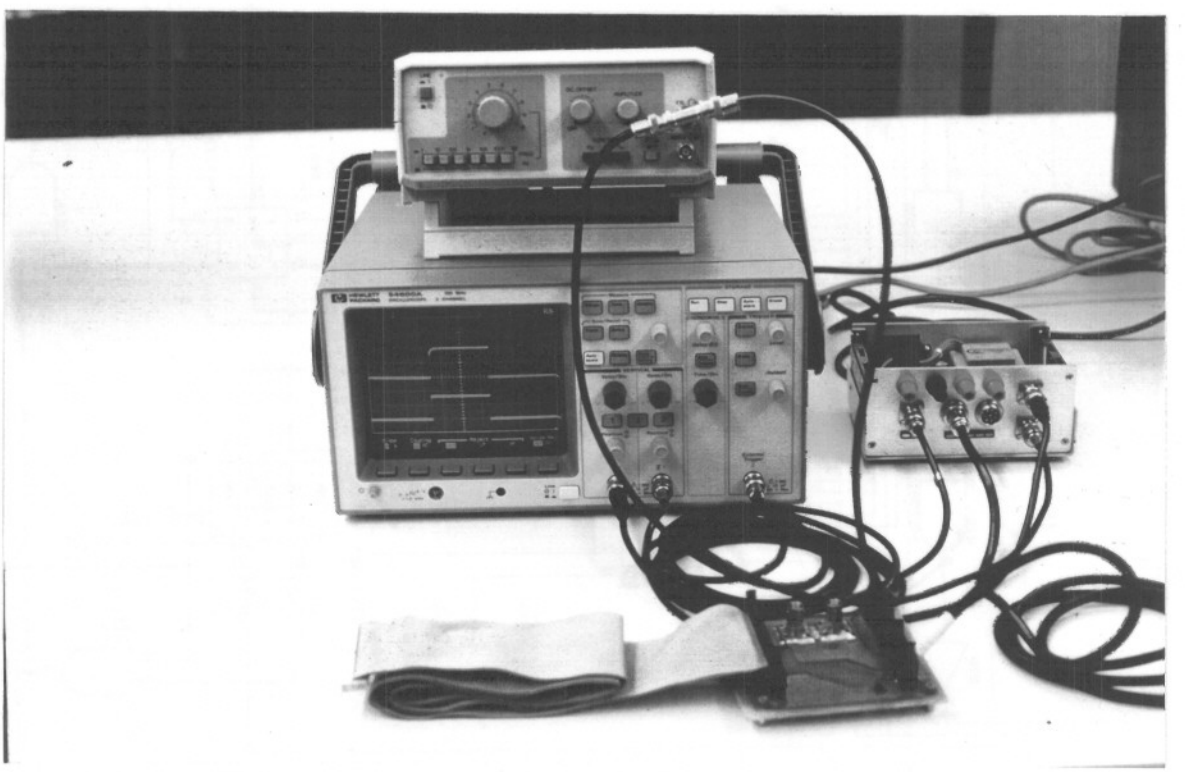

Fig.14 One of the synchronization units designed.

2.3.3 Test and measurement

Several tests have been conducted to measure the linearity of the digital potentiometers, the sync unit thermal drift and the range-resolved accuracy. During these tests, *DS1867-010* potentiometers were not available, and instead *DS1267-050* devices were used. *DS1267-050* is the *50 kΩ* volatile version (no EEPROM shadow memory) of the *DS1867-010*. Manufacturer's specs are very much the same for both series.

a) Linearity

When the device works as a voltage divider, absolute linearity is defined as the difference between the actual measured output voltage and the expected output voltage. Absolute linearity is given in terms of a minimum increment or expected output voltage when the wiper position is moved one position. A m*inimum increment (MI)* would equal

$$MI = \frac{V_{DD} - V_{EE}}{256} \tag{11}$$

where V_{DD} and V_{EE} are the positive and negative voltage supplies, respectively. The equation for absolute linearity *(AL)* is given next

$$AL = \frac{V_o(actual) - V_o(expected)}{MI} 100 \quad \% \tag{12}$$

Relative linearity *(RL)* is a measure of error between two adjacent wiper position points and is given in terms of *MI* by the following equation

$$RL = \frac{V_o(n+1) - V_o(n)}{MI} 100 \quad \% \tag{13}$$

Tab.6 is a summary of absolute linearity and relative linearity measurements versus wiper position for the *DS1267-050* at 25°C.

n	0	50	100	200	250
AL (%)	7.8	47.8	-27.0	-72.4	-22.0
RL (%)	12.2	7.0	10.6	17.4	7.0

Tab.6 Linearity measurements.

These values are slightly better than manufacturer's specifications of absolute and relative linearity ***(AL = ±0.75 LSB, RL = ± 0.30 LSB).***

b) Thermal drift

Fig.15 illustrates *OUT2* total drift after one hour of operation of the sync unit. With R_{ext} *= 50 kΩ* and C_{ext} *= 1.5 nF,* the unit synthesized *10.44-μs* delay and the drift was about

53 ns. This represents a delay error of 0.5 %. Comparing this value to the system resolution *(≈ 200 ns for R_{ext} = 50 kΩ)*, it represents less than 0.3 LSB.

Measurements have also been performed with C_{ext} = *330 pF, 720 pF and 1.5 nF*, giving a ***maximum drift of 1.2 LSB after one hour warm-up and 2 LSB after turn-on of the unit.*** The temperature coefficient of the digital resistor is *800 ppm/°C (typ)*.

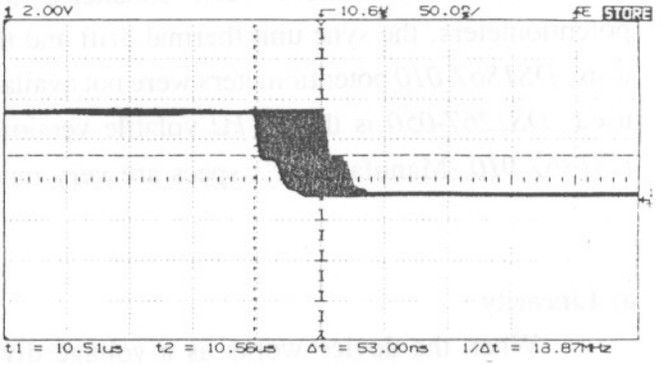

Fig.15 Thermal drift for a delay of 10.44 µs.

c) Accuracy

Accuracy of the timing unit is ultimately determined by linearity, tolerance of the $R_{ext}C_{ext}$ external timing components and wiper resistance *(typ. 400 Ω, max. 1000 Ω)*. Wiper resistance is not critical because it is always trimmed up to *2 kΩ* (this is the minimum specified value of R_{ext} for the *74121*) by the trimming potentiometer R_2 (Fig.12). Amongst linearity and tolerance, capacity tolerance is the most concerning factor, even though these potentiometers have ± *20-%* tolerance. Since the timing delay only depends on the product $R_{ext}C_{ext}$ (eq.(7)), a good method to remove tolerance effects on system accuracy is to measure end-to-end potentiomenter resistance and plot the timing delay versus the cursor position. Then, the optimum C_{ext}, $E(C_{ext})$ that yields minimum mean-square error can be calculated. Once this is done, $E(C_{ext})$ is the true capacitance. If that value is programmed in the control unit, subsequent plots of time delay versus wiper position will leave linearity as the only error source. In Fig.16 such error plot is shown for C_{ext} = *1.5 nF,* which yields $E(C_{ext})$ = *1.431 nF*. Absolute linearity in delay is ±*82 % (≈ ±1 LSB)*. During the tests conducted only one *DS1667-050* unit (*50 kΩ* version) was used. To comply with the maximum R_{ext} specification for the *74121* timer, the maximum wiper position was limited to n=*170*. Nearby this position, the error increases because of *74121* nonlinearities, which are thought to be caused by the parasitic capacitance of the *DS1667-050* potentiometers.

In Fig.17 one can see a measure of the delay increment between two adjacent wiper positions. Comparison with the expected delay *(50 kΩ/256·1.431 nF·ln2 = 194 ns)* gives a measurement of the delay relative linearity (RL). It yields *RL* = ±*9 % (≈ ±0.1 %)*. Further measurements with different capacitive values also yielded ***AL < 1.6 LSB*** and ***RL < 0.1 LSB***. Note that the RL value is overridden by the manufacturer's specs given in (a).

Summing up points (a),(b),(c), the sync unit has the accuracy shown in Tab.7.

AL ≈ 2.8 LSB (1 h. warm-up), 3.6 LSB (turn-on); RL ≈ 0.3 LSB

Tab.7 Sync unit accuracy including thermal drifts.

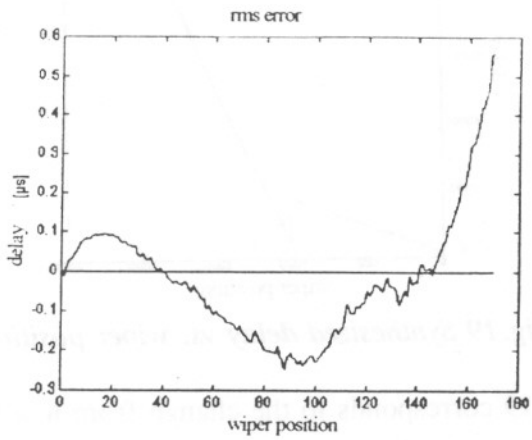

Fig.16 Absolute linearity measurement.

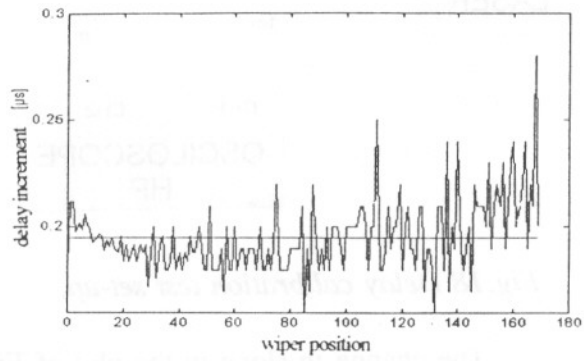

Fig.17 Relative linearity measurement.

2.3.4 Calibration model for the sync unit

In the preceding section, it has been shown that the unit has reasonable good performance when the multiplexed capacitance, C_{ext}, has been calibrated. Then, performance is only limited by nonlinearities of the digital potentiometers and monostable timers. These errors can be compensated if the control unit incorporates a regression table that relates wiper position of each potentiometer and scale to the delay that is to be synthesized.

Fig.18 shows the calibration set-up used to run the calibration program. If the oscilloscope has a GPIB interface, the delay between the Advanced Sync Output and OUT2 can directly be read by the control unit. Fig.19 shows the delay synthesized for each of the 2048 wiper positions (4 potentiometer x 256 positions each x 2 scales). This plot can be regressed by eight lines (one for each potentiometer and scale) of the form

$$T_{i,j} = k_1 n_{i,j} + k_2 \qquad (14)$$

where $n_{i,j}=0..255$ is the position of wiper i in the scale j (low or normal range) with all the other potentiometers set to $n=255$.

SCALE	low range (1 LSB equals $\Delta T \approx 1.65$ ns, $\Delta R \approx 0.25$m)				normal range (1 LSB equals $\Delta T \approx 10$ns, $\Delta R \approx 1.5$m)			
POT	1	2	3	4	1	2	3	4
k_1	1.7495	1.6499	1.6125	1.6192	8.9512	9.8524	10.522	10.494
k_2	157.23	609.17	1027.0	1442.5	665.07	2945.0	5462.1	8171.5
ERROR	4.5 LSB	1.8 LSB	1.9 LSB	2.2 LSB	0.3 LSB	1.8 LSB	0.8 LSB	1.1 LSB

Tab.8 Look-up regression table in the control unit.

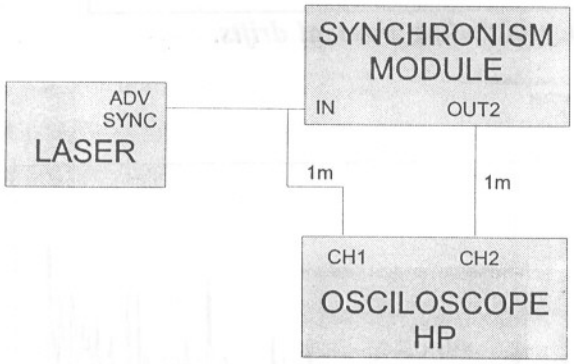

Fig.18 Delay calibration test set-up.

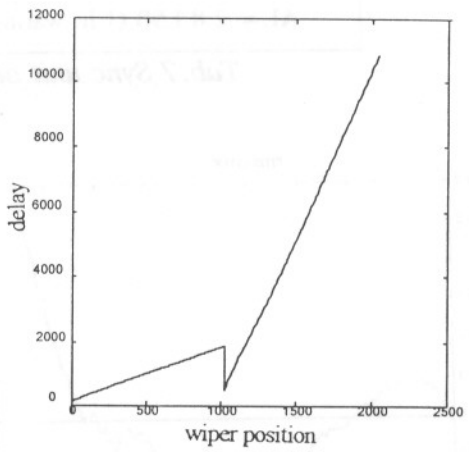

Fig.19 Synthesized delay vs. wiper position.

The change in slope in the plot of Fig.19 corresponds to the change from low to normal scale. Note that for a small interval, the sync unit can synthesize the same delays in both scales but, of course, with different resolutions. Note also, that maximum and minimum delays are different from those expected in Tab.4, because of the capacity tolerance. Tab.8 shows the regression table along with delay errors in LSB units.

2.4 Microprocessor-based synchronization unit

The second unit, which is still undergoing calibration tests in our laboratories, is based on a *27-MHz 87C51* microprocessor. The buffer is mapped into the microprocessor's RAM and timers T_1 and T_2 have been implemented using *74F163* fast-speed counters controlled by a *40-MHz* quartz crystal. Compared to the RC-timing unit this new unit features *very low thermal drift and much better linearity,* which results in improved accuracy. Thermal drift is greatly reduced because timing resistors have been replaced by a quartz crystal. The large improvement in linearity comes from the substitution of monostable timers by fast-speed counters controlled by crystal. Moreover, by cascading three counters in the T_1 timer stage (see block *B* in the circuit diagram of Fig.20) a single scale is enough to span the whole $R_{min}{}^{s}$ range.

The functional diagram of this unit (as far as it concerns the timing functions implemented) is exactly the same as the one given in Fig.9. Handshake lines with the control unit are the same as before and the only change lies in the data word structure. The *40-bit word* that was used for the buffered sync unit of Sec.2.3, is now replaced by a *14-bit word.* 14 bits are enough to program timer T_1 (3 counters x 4 bits each), receiver state (1 bit) and latch (1 bit). Tab.9 gives a brief outline of the unit along with its expected features. A circuit schematic of the unit is shown in Fig.20. Functional circuit blocks are boxed and indicated with capital letters. These blocks are:

- (A) 87C51 Microcontroller,
- (B) T_1-timer including three 74F163 fast-counters,
- (C) T_2-timer including two 74F163 fast-counters,
- (D) flip-flops used to synchronize the Adv Sync signal to the *40-MHz* base clock and to generate OUT_1 and OUT_2 signals,
- (E) combinational logic and,
- (F) driving logic for LEDs.

System operation is based on an interruption policy. Interruptions are triggered by the Advanced Sync signal and PC requests to send data. PC access time and *1-ms* listen window are controlled by interal timers of the microprocessor.

MICROPROCESSOR-BASED SYNC UNIT		
Externally generated delays		
T_1 delay	12-bit count	40-MHz base clock (74F163)
Resolution:	ΔT = 25 ns (eq.(10))	
Delay range:	$T_{1,min}$ = 25 ns (1 count)	$T_{1,max}$ = 102.40 μs (2^{12} counts)→ 15.36 km
T_2 delay	8-bit count	same base clock (74F163)
Resolution:	ΔT = 25 ns	
Delay range:	$T_{2,min}$ = 25 ns (1 count)	$T_{2,max}$ = 6.40 μs (2^8 counts)
Internally generated delays		
1-ms gate (listen window), READY1 and LATCH		
Controlled by microprocessor timers.		27-MHz base clock (87C51)

Tab.9 Microprocessor-based sync unit performance.

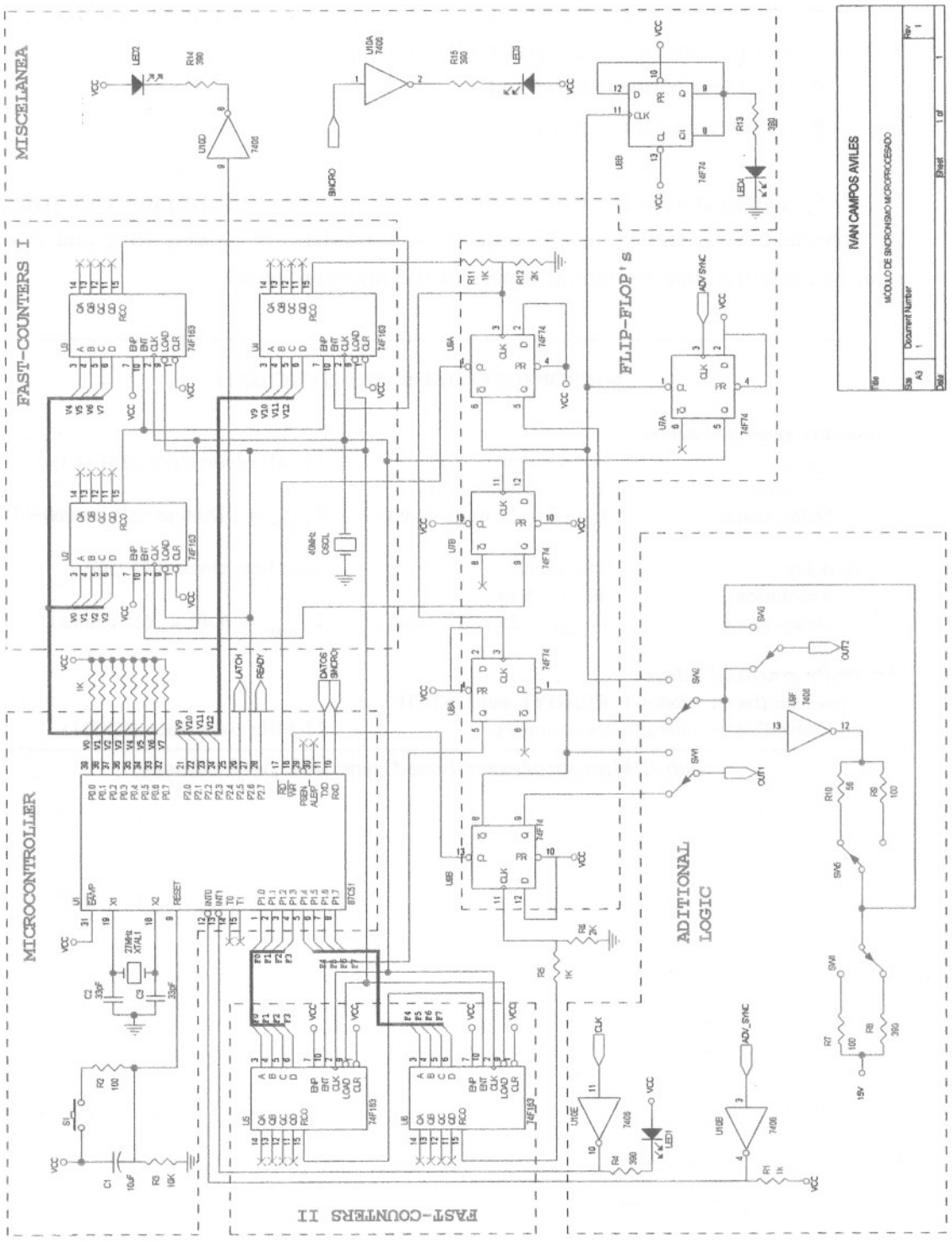

Fig. 20 Sync unit microprocessor-based circuit.

3. THE CONTROL UNIT

3.1 The virtual instrument approach

LabVIEW software is a graphical alternative to conventional programming. It is a graphic language designed for instrumentation and is equipped with all the tools that are needed for process monitoring and process control applications. ***In LabVIEW, icons are connected and assembled to build programs, called virtual instruments (VIs), instead of writing text-based programs (e.g. C code).***

A LabVIEW VI consists of a *front panel,* a *block diagram,* and an *icon/connector.* The front panel is the user interface, the block diagram is the *VI* source code, and the icon/connector is the calling interface to other icons. The front panel of the control program of the lidar system is shown in Fig.21. It arranges common components such as meters, knobs, switches and a display where the lidar signal is displayed.

Each element in the front panel also appears in the block diagram as a *terminal.* A block diagram resembles a traditional engineering flowchart and contains icons representing input/output (I/O) functions, computational functions, and analysis functions. A worthy advantage is that I/O elements of the diagram communicate directly with the plug-in data acquisition cards *(PC-LPM-16 and GaGe CompuScope 1012)* and GPIB board. Computational components such as adders, derivators, etc. perform arithmetic and other operations. Variables are passed by connecting these block diagram icons together with *lines or wires.* In Fig.22 the top-level diagram of the lidar control program is shown. As long as lower icons are opened, information is more and more specific until basic procedures are reached (e.g open port, read/write port instructions).

The front panel is the interactive interface for the person who is controlling the lidar in the control room. When the VI is running, one can click a switch to turn-on the laser, move a slide to change the minimum exploring range, tweak a knob to change the laser lamp energy, or enter a new display range from the keyboard. The panel response is virtually immediate (depends on the CPU load), providing a real-time feedback from the lidar system. In the design of the front panel participated many people from the lidar team.

Parallelism is an important feature in LabVIEW programming, and that was a good point to make a decision in favour of this software. That is how parallelism is achieved:

The function icons and structures explained are referred collectively as *nodes.* Each node begins operating when data is available at all of its inputs. For instance, in the diagram of Fig.22, the synchronism unit, which is depicted as a clock, is a node. When the node finishes executing, it produces data for all of its outputs. This *data-driven method* of execution is called *control dataflow.* Because the execution order in LabVIEW is determined by the flow of data between nodes and not by sequential instructions (e.g. conventional C programming) the control program has multiple data paths and simultaneous operations. As a result, the control program executes independent data paths and VIs simultaneously.

The control program is modular by design. That is, VIs are subVIs from the upper-level block diagram. The control program contains about a hundred icons one inside the other. The program has been built in a bottom-up approach. Low level subVIs have been used as nodes to build increasingly sophisticated layers of VIs. Thanks to this modular hierarchy, it is possible to design, modify, and interchange VIs. That is how different versions of the synchronization unit can easily be incorporated into the control program. ***Each synchronization unit has its icon counterpart and by means of software switches one unit can relay another in case of serious failure or damage.*** Each icon contains the operation protocol. Note that this hierarchy also enables to reuse many icons for new lidar applications. In addition, the control program has context-sensitive user interfaces that are configured to open automatically to give warning information (e.g. *Warning: Laser interlock-fault. Please,...).*

Fig.23 shows part of the modular hierarchy of the control program.

3.2 Acquisition and control cards

Built-in libraries for GPIB, RS-232 and plug-in acquisition boards are also included in LabVIEW. Nowadays, many acquisition card manufacturers strive to provide the user with LabView libraries for their cards. That is the case of the *CompuScope 1012* card, which is the card used for data acquistion in the lidar system. Using the built-in libraries, raw-data is converted into meaningful results in the *I/O icons.*

Tab.10 summarizes the specifications for the multifunction I/O board PC-LPM-16 and the lidar acquisition card CompuScope 1012. This table is intended to serve as a reference for other chapters.

I/O INTERFACE CARDS

LIDAR DATA ACQUISITION **CompuScope 1012-512K** from Gage Applied Sciences Inc.

Acquisition

Channels:	2 at 10 Msps (max) or 1 at 20 Msps (max);	12 bits
Ranges:	±100 mV, ±200 mV, ±500 mV, ±1 V, ±5 V.	
SNR:	65 dB at 10 Msps (1 MHz input in ±1 V range) (see $\sigma_{i,AD}$ in Chap.3)	
Memory Depth:	512 K and uses DMA	

Trigger

256 levels (positive or negative slope); Pre, Mid, or Post-trigger
External may be AC or DC coupled, 10-MHz bandwidth

MULTIFUNCTION I/O **PC-LPM-16** (XT/AT computer bus) from National Instruments

Analog Input *Intended to implement alarm module and sample laser output energy.*

Channels:	16 single-ended channels (±2.5, ±5 V);	12 bits
Sampling rate:	50 ksps (round-robin scan frequency).	

Digital I/O *Lidar bus interface.*

Channels:	8 inputs / 8 outputs

Tab.10 I/O interface cards of the control unit.

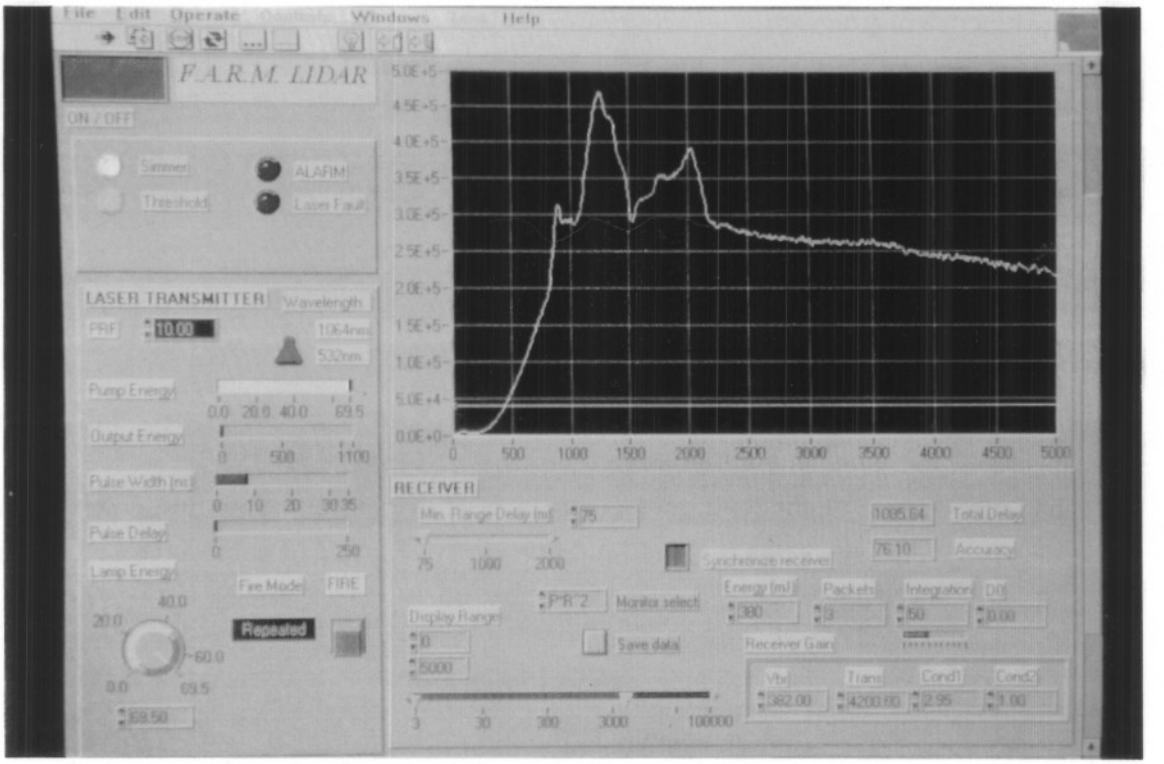

Fig.21 Front panel of the control program.

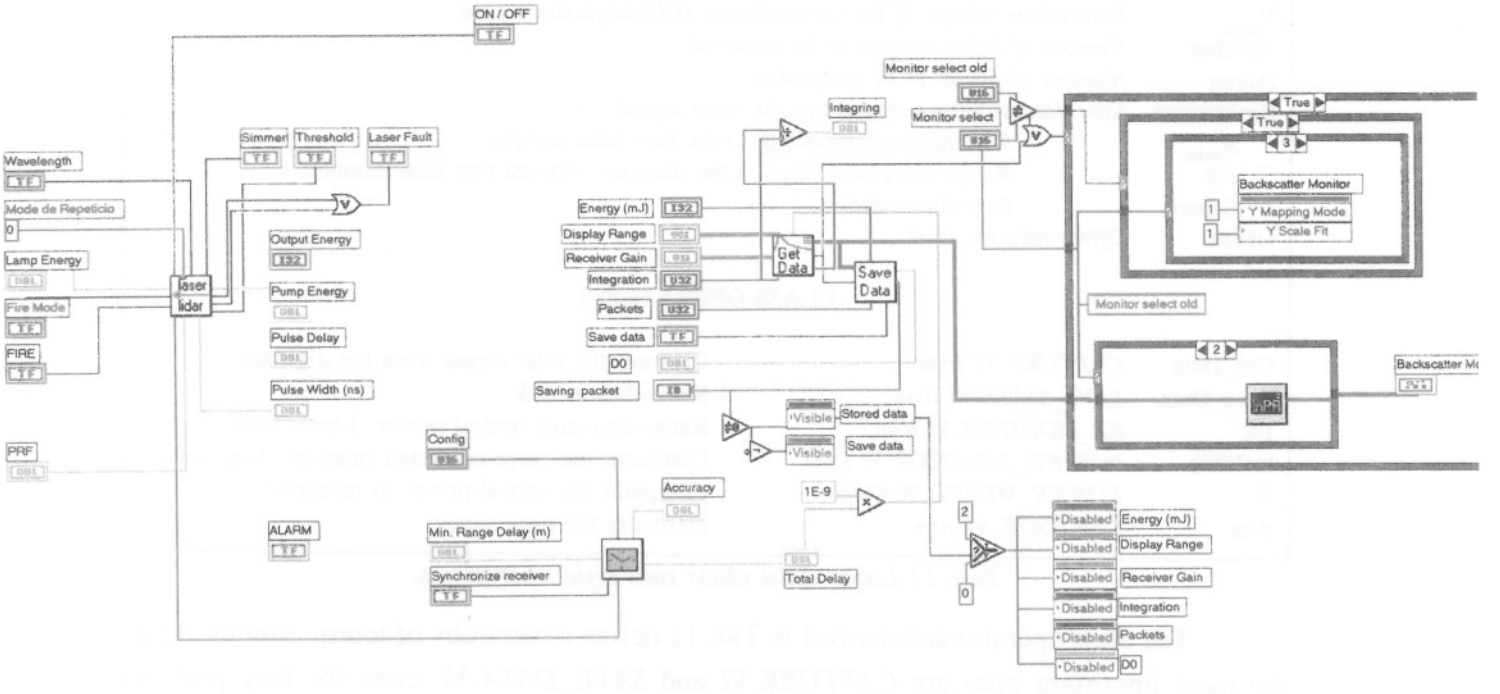

Fig.22 Block-diagram of the control program showing nodes.

3.3 The control program

The VI that controls the lidar system is divided into three main blocks: *laser control, sync module control and acquisition and data display*. Raw-data preprocessing is performed by the acquisition and data display VI and it is discussed next in Sect.3.3.1. The sync module control is responsible for the time-range calibration of the system and it is discussed in Sect.3.3.2.

3.3.1 Raw-data preprocessing

In LabVIEW data is organized into classes. A class is a data type with its own data structure. Each class is defined by its structure and related operations.

The lidar class is the top class of the control program. Operations with this class are performed by top-level icons (VIs) that contain a myriad of sub-VIs. Tab.11 describes the lidar signal class.

DATA STRUCTURE		
Receiver	*Receiver parameter structure*	
V_{BR}	APD bias voltage. An interpolation procedure is used to compute the multiplication gain, M, from V_{BR}.	
Trans	Transimpedance gain.	
Cond1	First stage conditioning gain.	
Cond2	Second stage conditioning gain.	
V_{max}	*Saturation voltage of the CompuScope 1012 acquisition card*	
Number	*Number of lidar samples to be acquired*	
Pulses	*Number of pulses to be integrated*	
Backscatter	*Raw-data structure containing the lidar signal*	
R_{min}	Distance corresponding to the first lidar sample.	
ΔR	Range increment. This is the distance between two lidar samples.	
Screen	Raw-data samples.	
Offset	*Offset receiver level*	
CLASS OPERATIONS		
Get_Data	*CAPTURE.VI icon*	Captures the lidar signal from the digitizer.
Save_Data	*SAVE_DATA.VI icon*	Saves data to disk.
PR^2	*R2_MONITOR.VI icon*	Range-corrected optical power. Linear scale.
$\ln(PR^2)$	*ln(P*R2)_MONITOR.VI icon*	Computes the range-corrected function. Log scale.
P	*POWER_MONITOR.VI icon*	Computes the optical power in reception.
d/dt	*DERIVATE.VI icon*	Derivates the lidar signal.

Tab.11 Lidar data class and type operations.

The class operations described in Tab.11 define a hierarchy of icons. Among them, the most important ones are *CAPTURE.VI* and *SAVE_DATA.VI* icons for they perform important preprocessing operations. *CAPTURE.VI* icon performs pulse integration of the lidar signal and outputs a data type that contains raw-data samples, receiver gain, and integration procedure. With this information, it is possible to compute the backscattered

optical power in absolute terms, since from the data structure the net responsivity of the receiving chain is readily available. This icon is implemented with four sub-VIs (see the hierarchy diagram of Fig.23), two of which deserve especial attention.

The first sub-VI is the *SCREEN.VI* icon. This virtual instrument is responsible for the CompuScope acquisition card. It carries out display monitoring of the lidar signal and offset compensation. It has been discussed in Chap.4 that in the absence of lidar signal, the output of the lidar receiver is the composite offset from receiver op amp offsets and photometric background offset. To compensate both kinds of offsets data acquisition is performed in two DMA sequences. In the first one, a data segment comprising *100 km* is acquired. This is theuseful range-return lidar data segment. The second DMA acquires *64 samples* corresponding to the range interval between *99.9 km* and *101.2 km*. These samples are averaged together and since, at such long ranges the lidar signal is well below the system noise (i.e. only steady-state photometric background is present), the composite offset is retrieved. In addition, since this operation is performed periodically for each data packet, *offset thermal-drift is compensated as well.*

The second sub-VI from *ACQUIRE.VI* is called *INTEGRATOR.VI*. As its name suggests, it performs pulse integration of *N* lidar return-signals. The operating principle is quite simple: the data segment from each return-pulse is stored in a buffer until the *Nth-pulse* arrives. This pulse starts data integration by summing all the segments, sample by sample, and by dividing the sum them by *N*. The data segment that results from such integration is called a *packet*. Both the number of pulses per integration and number of packets can be chosen from the front panel.

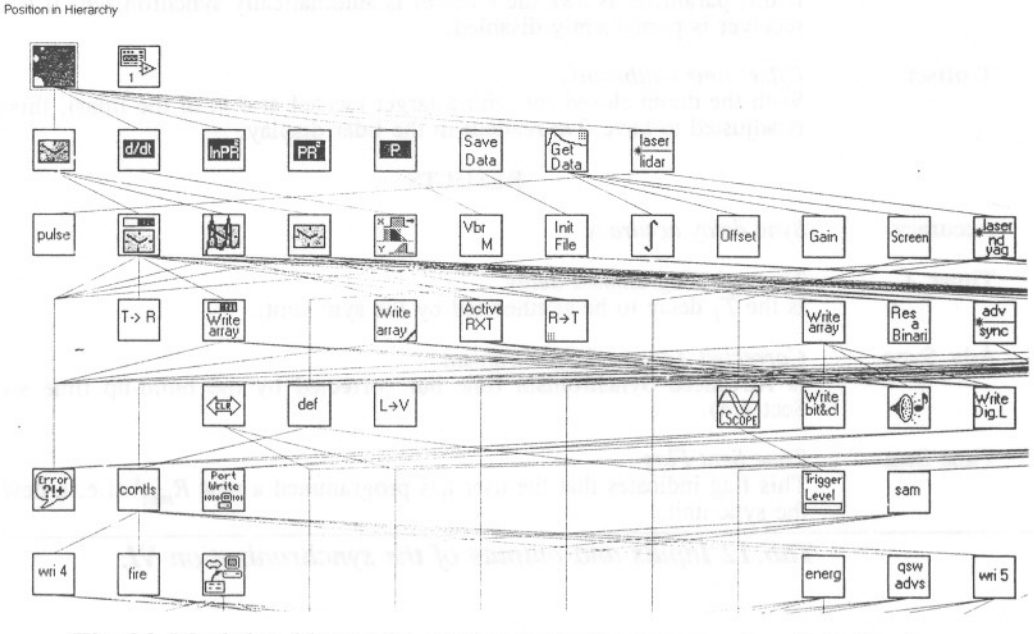

Fig.23 Modular hierarchy of the control program (partial view).

SAVE_DATA.VI saves data following *MATLAB .mat-format*. Information is saved in two files: a header file in *MATLAB .m-format,* which contains lidar system parameters, preprocessing parameters and a field for free commentaries; and a second file that contains lidar raw-data in *.out-format*. The *.m file* is organized in such a way that once it is called from the MATLAB prompt, it automatically loads all system parameters and makes a call to the *.out-file*. As a result, lidar data is loaded into MATLAB's working environment in form of data matrix, whose rows contain lidar packets and whose columns contain the lidar samples belonging to each packet.

3.3.2 Sync module control

The sync module virtual instrument (Fig.24) controls the synchronization unit. Tab.12 lists the main inputs and outputs of this VI. It performs two basic functions:

- Computation of the *Corrected Advanced Synchronism* of Tab.12 according to the build-up correction given by eq.(20) in Sect.4.4 and,
- Computation of the *Timer_1 Delay* of Tab.12.

Note that if the build-up correction is enabled, the sync module control will output a different T_1 delay value every PRP, depending on build-up voltage fluctuations.

	PARAMETERS
R_{min}	*Minimum range $R_{min}{}^{s}$* $R_{min}{}^{s}$ indicates the range where the exploring window begins.
Enable	*Receiver enable mode* If this parameter is *true* the receiver is automatically synchronized, if it is *false* the receiver is permanently disabled.
T-offset	*Offset time calibration* With the doom closed (or with a target located at *0 m* of the lidar), this parameter is adjusted to have *0 m* readout in the lidar display.
	RESULTS
Accuracy	*Sync delay accuracy*
Timer_1	*Timer_1 programmed delay* Is the T_1 delay to be synthesized by the sync unit.
Adv_Sync	*Corrected Advanced Synchronism* Is Advanced Synchronism time but corrected by the build-up time signal. (See Sect.4.4).
Time Sent	*Time Sent Flag* This flag indicates that the user has programmed a new $R_{min}{}^{s}$ (i.e. a new delay) in the sync unit.

Tab.12 Inputs and outputs of the synchronization VI.

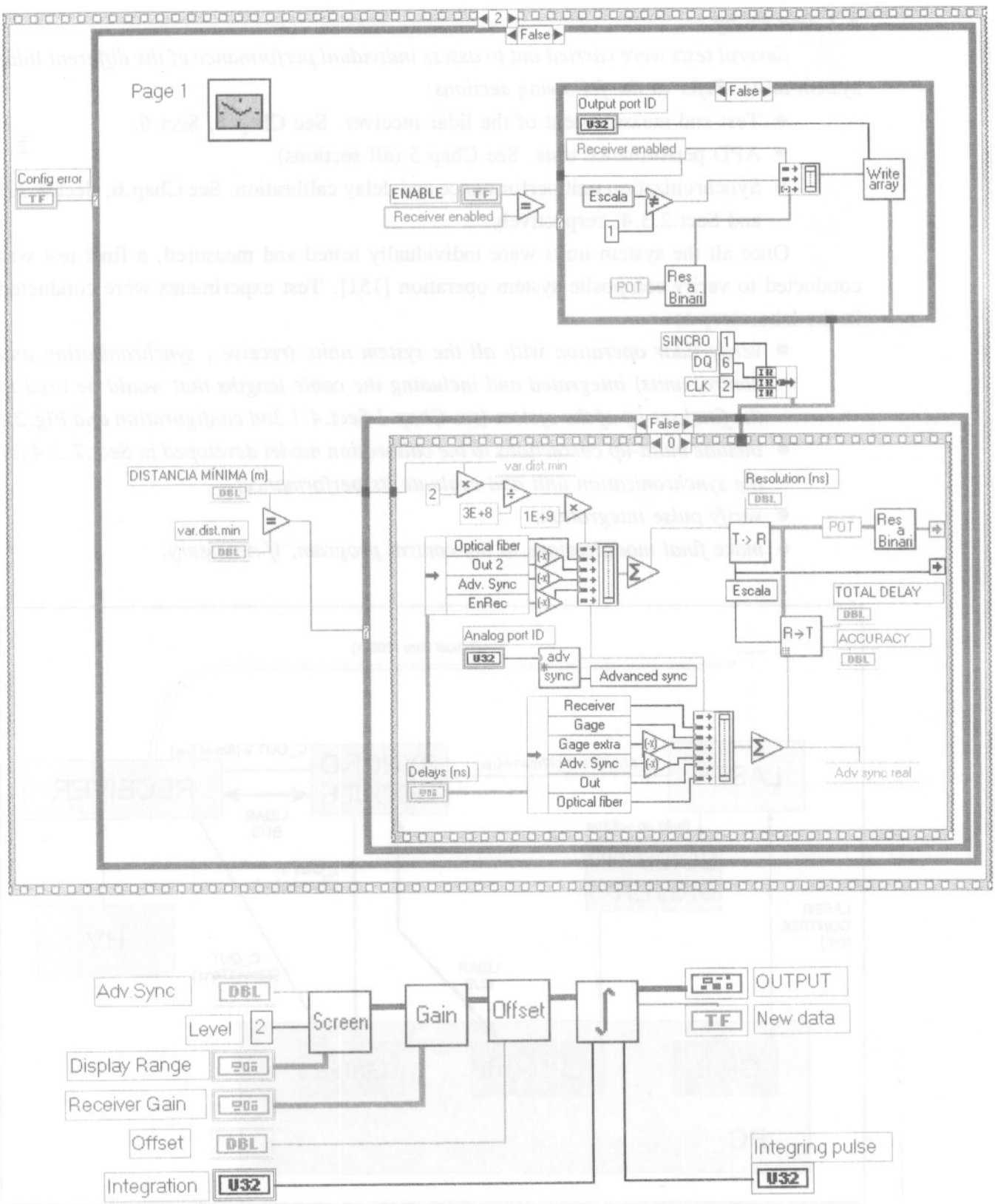

Fig. 24 Synchronization VI (top) and Get_Data VI (bottom).

4. SYSTEM TEST EXPERIMENTS

4.1 Test set-up

Several tests were carried out to assess individual performance of the different lidar system units. Refer to the following sections:

- Test and measurement of the lidar receiver. See Chap.4, Sect.6.
- APD performance tests. See Chap.5 (all sections).
- Synchronization unit performance and delay calibration. See Chap.6, Sect.2.3.3 and Sect.2.3.4, respectively.

Once all the system units were individually tested and measured, a final test was conducted to verify composite system operation [151]. Test experiments were conducted in the laboratory to

- *verify lidar operation with all the system units (receiver, synchronization and control units) integrated and including the cable lengths that would be used in the final set-up of the system (see Chap.1 Sect.4.1 2nd configuration and Fig.2);*
- *include build-up corrections to the calibration model developed in Sect.2.3.4 for the synchronization unit and evaluate its performance;*
- *verify pulse integration;*
- *make final modifications to the control program, if necessary.*

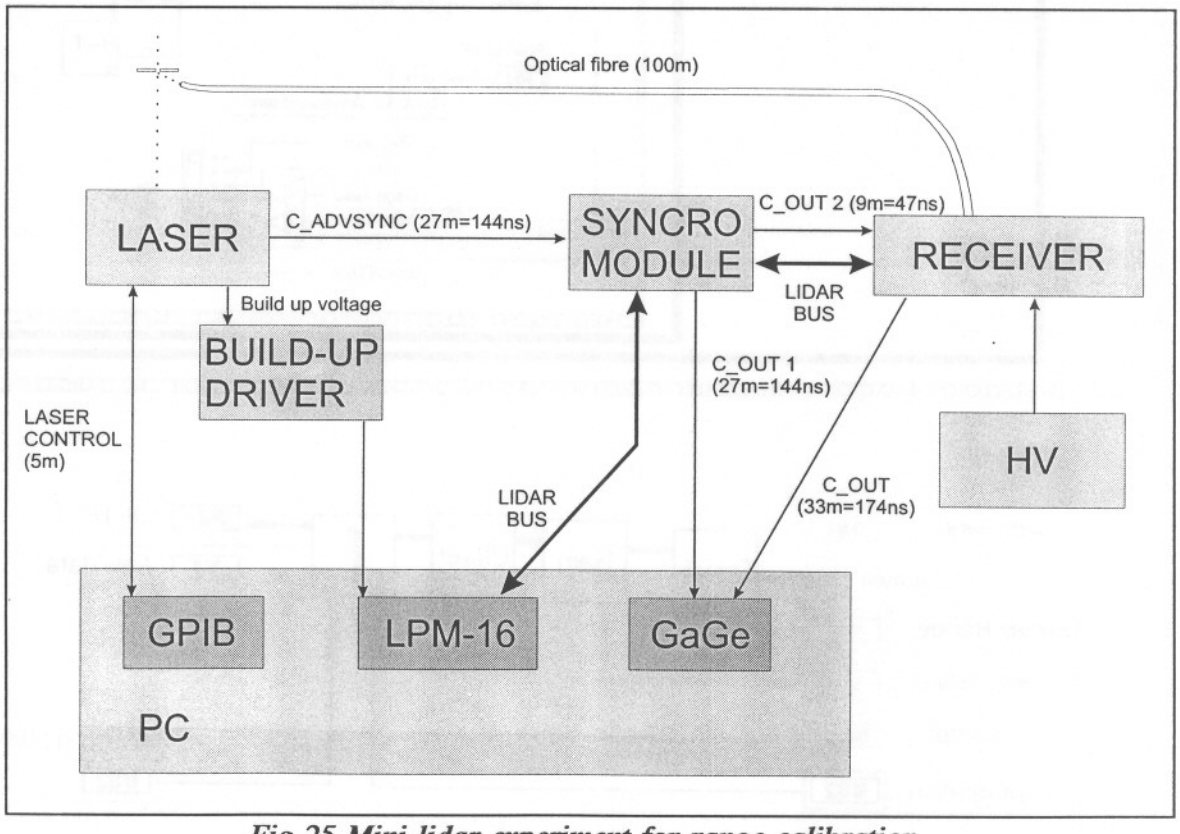

Fig.25 Mini-lidar experiment for range calibration.

The test set-up is sketched in Fig.25. In the set-up cable lengths were the same as those that would be used in the final set-up of the system (Chap.1 Sect.4.1 2nd configuration and Fig.2). At the laser's end, light is scattered by means of white paper square situated in front of the laser and it is collected by a *50-μm* fibre (See Fig.26). Since according to the specifications of Tab.2 the minimum range that the synchronization unit can synthesize is $R_{min}{}^{s} = 100\ m$, the lidar signal trip delay was simulated using the *100-m* fibre. At the other fibre's end, the fibre connector was approached about *5 cm* to the camera, where the lidar receiver was mounted (Fig.27).

4.2 Performance

First the experiment was performed at a laser wavelength of $\lambda = 532\ nm$ using an output energy of *1 mJ*. The successful result of this experiment is shown in Fig.28, where the oscilloscope's screen is displayed. In the figure, the end of the disable window (flat signal) and the beginning of the listen window (typical lidar pulse) can clearly be appreciated. Ringing effects lasting for half a division are also evident. With *200 ns/div* base time in the oscilloscope, this means a ringing period of *100 ns,* which is in close agreement to the time length of the receiver impulse response *(109 ns for a bandwidth of 9.2 MHz)*. In the same figure and after the large lidar-return signal, a second return can also be spotted. A later test showed that what seemed a ringing effect was in fact a second-order reflection. Inspection of the lidar signal in the backscatter display of the control unit (Fig.21) helped calibration of the T_2-delay in the synchronization unit (Fig.9), which compensates for different cable lengths between branches OUT_1 and OUT_2. Note that in Fig.21 the lidar signal appears at a negative range (approximately *-100 m)*. By adjusting T_2 is was possible to compensate the different delays between outputs OUT_2 (receiver sync signal) and OUT_1 (acquisition trigger). Recall that delay *T1* was calibrated by means of the test set up of Fig.18 and the procedure described in Sect.2.3.4. A straightforward link-budget for this experiment is given in Sect.4.3.

The same experiments was repeated at *1064-nm* wavelength. Pointing was achieved by maximization of the lidar signal in the control unit display (Fig.21).

Another test was conducted based on the same principle, but this time the optical fibre and the camera were replaced by a Celestron telescope, where the receiver was mounted. With this set-up the configuration was exactly the same as the one that would be used for the atmospheric experiments except that the actual experiment was carried out in the closed environment of the laboratory. Since the minimum distance that the telescope can focus is about *25 m*, the telescope was aimed at a door handle, where very dim reflections from multiple scattered light could be spotted. Fig.29 shows a photograph of the experiment, which also ended with successful results.

4.3 Link-budget

A rough link-budget based on radiance studies was performed to corroborate the order of magnitude of the lidar signal received. It can be summarized as follows:

When the laser shots illuminated the white paper target, a very bright scatter appeared in front of it coming out in all directions. (In Fig.26, only the laser spot can be distinguished because the exposure time of the photograph has largely been reduced for artistic purposes).

The radiance L_E arriving at the fibre optics is equal to the radiant flux [$J \cdot s^{-1}$] per unit area and solid angle:

$$L_E = \frac{E}{\tau_l A_e \Omega_e} \qquad \left[\frac{W}{m^2 sr}\right] \tag{15}$$

where

E is the laser pulse energy *(1 mJ)*,

τ_l is laser pulse duration *(10 ns)*,

A_e is the emitting area of the white paper *(6 x 8 cm)* and,

Ω_e is the solid angle of emission *(2π sr)*.

Among these parameters, the solid angle of emission is the most difficult one to guess. When the experiment was performed it was seen that part of the light scattered from the white paper suffered a second scatter in the front cover of the laser, which reinforced the scattering. In addition, a matt piece of white paper is often considered a Lambertian emitter. Yet, Lambert's law is not always fulfilled. The best Lambert source is a blackbody emitter. An extremely poor Lambert source is a laser beam since the emitted light forms a strongly directional beam. Both effects considered, multiple scattering and Lambert's law, it has been thought that a reasonable approximation would be to assume nearly uniform radiation into the solid angle $\Omega_e = 2\pi$ *sr*. Substitution of the values given above into eq.(15) yields

$$L = 3.3 \cdot 10^6 \ W m^{-2} sr^{-1}$$

The radiant flux, P_1 *[W]* from the paper that reaches the fibre may be expressed as

$$P_1 = L_e \Omega_r A_r \qquad [W] \tag{16}$$

where

L_E is the radiance computed above,

Ωr is the receiving solid angle of the fibre optics and,

A_r is the fibre optics receiving area.

For each point of the receiving area of the fibre, there is an acceptance cone, whose opening α is directly related to the numerical aperture, *NA*. The solid angle of this cone, Ω_r can be expressed as

$$\Omega_r = \pi \sin^2 \alpha = \pi NA^2 \tag{17}$$

Assuming a typical numerical aperture $NA = 0.17$ ($\alpha = 10°$) yields

$$P_1 = 0.62\ mW$$

At the other fibre's end (see Fig.27) light from the opening cone of the fibre is projected onto the photodiode active area of the receiver. At this point much light is lost due to overspill. Overspill loss can be determined by the ratio of the APD active area to the illumination area. The APD active area, or equivalently its diameter, can be known from the manufacturer's specs and the diameter of the illumination area can be computed from fibre-to-camera distance and the opening angle of the fibre. Mathematically,

$$Loss = \left(\frac{D_{APD}}{2dtg\alpha} \right)^2 \tag{18}$$

where

D_{APD} is the diameter of the active area of the APD *(0.8 mm)*,
d is the distance between the fibre's end and the active area *(d=5 cm)* and,
α is the opening angle of the fibre *(NA = sinα = 0.17)*.

Substitution of these values into eq.(18) enables to compute the effective power that illuminates the active area of the APD, which yields

$$P_2 = P_1 \cdot loss = 1.3\ \mu W$$

Finally, this optical power can be related to the voltage output readout in the oscilloscope by knowing the voltage responsitivy of the receiver. The gain settings were: multiplication gain, $M = 120$, transimpedance gain, $G_T = 4000\ \Omega$ and conditioning gain $G_A = 10\ V/V$. Since the APD typical intrinsic responsivity is $R_{io} = 0.3\ A/W$, the voltage responsivity, R_v can be computed as

$$R_v = R_{io} G_T G_A \tag{19}$$

which yields $R_v = 1.44 \cdot 10^6\ V/W$. Consequently, the voltage readout would be

$$V_{read} = 1.8\ V$$

That would be the expected voltage readout in the oscilloscope screen, or at least the order of magnitude of the expected value. By checking this estimation with the oscilloscope readout in Fig.28 *(6 div x 130 mV/div = 0.78 V)*, we see that this result is in close agreement to the estimation given above and hence this link-budged is corroborated by the measurement.

It is time now we revised if assuming Lambertian behaviour could improve this result. We note that if in Fig.26, a cosine law dependence were assumed with a fibre-to-paper tilting angle $\theta = \pi/3$, the voltage readout would have been $1.8V \cdot cos(\pi/3) = 0.9\ V$, which results in closer agreement to the voltage readout measured.

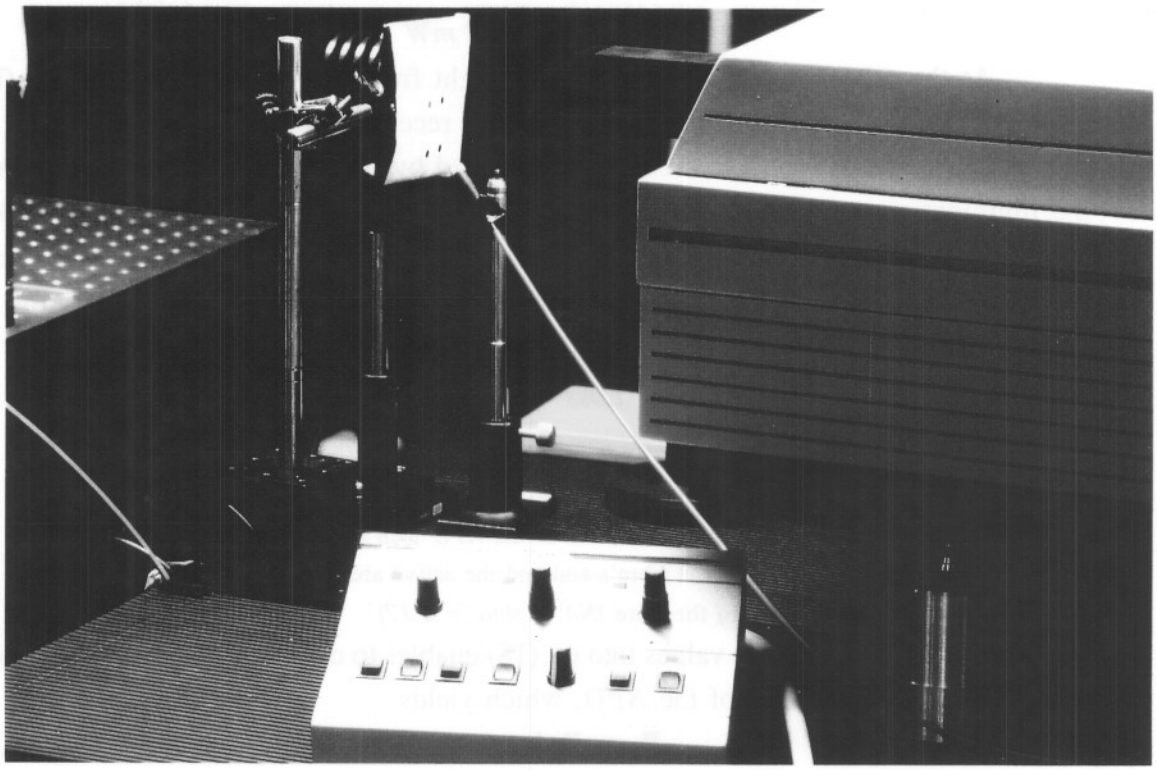

Fig.26 Optical fibre collecting light scattered near the laser.

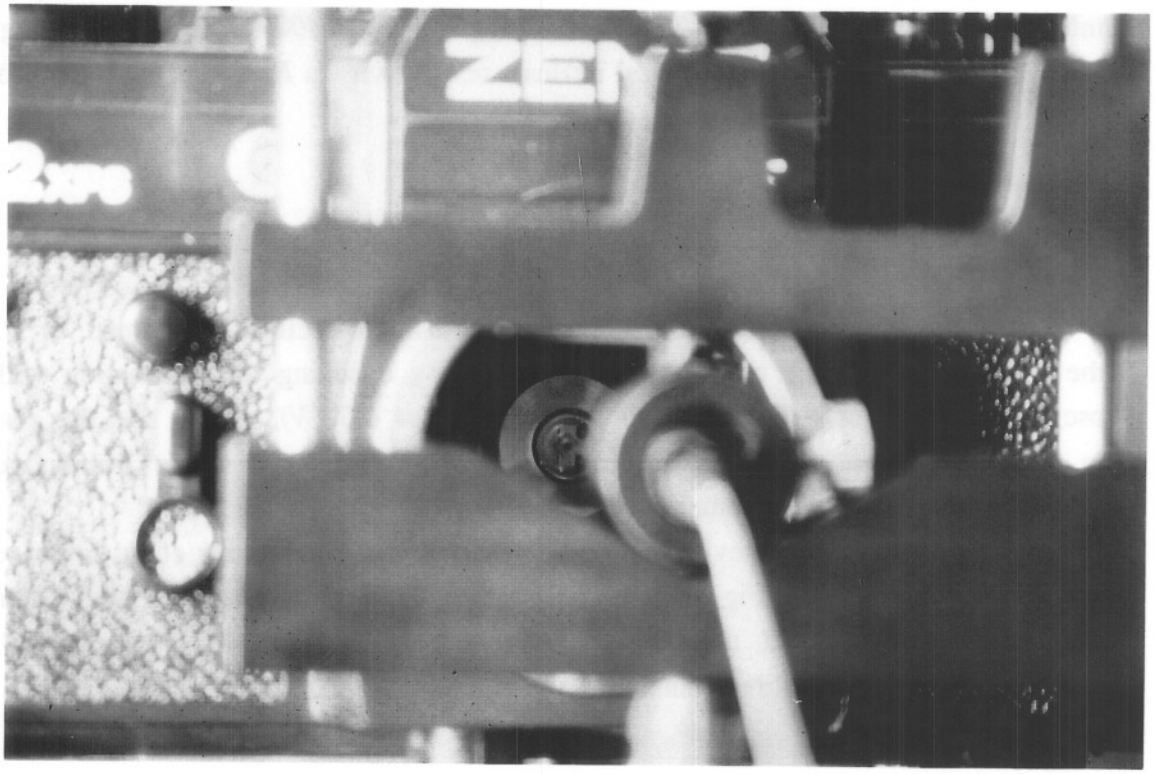

Fig.27 Lidar receiver mounted in the camera and collecting light from the fibre's end.

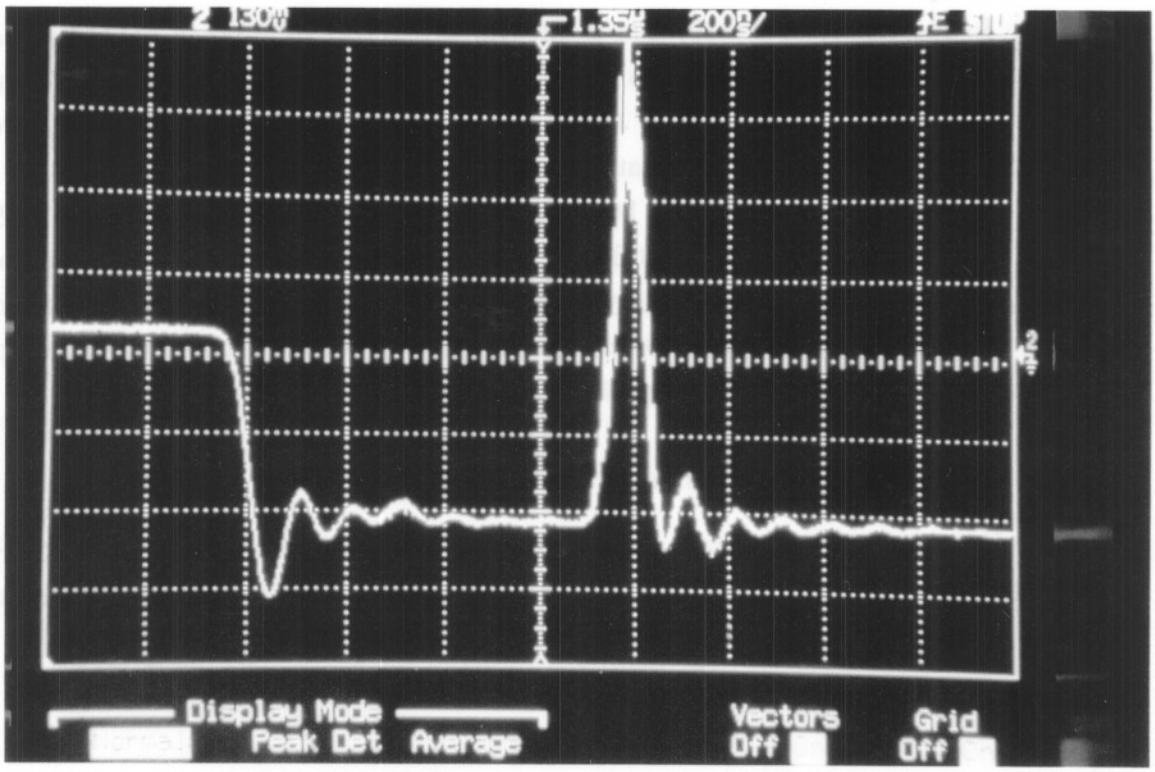

Fig. 28 Lidar signal in reception showing the disable window.

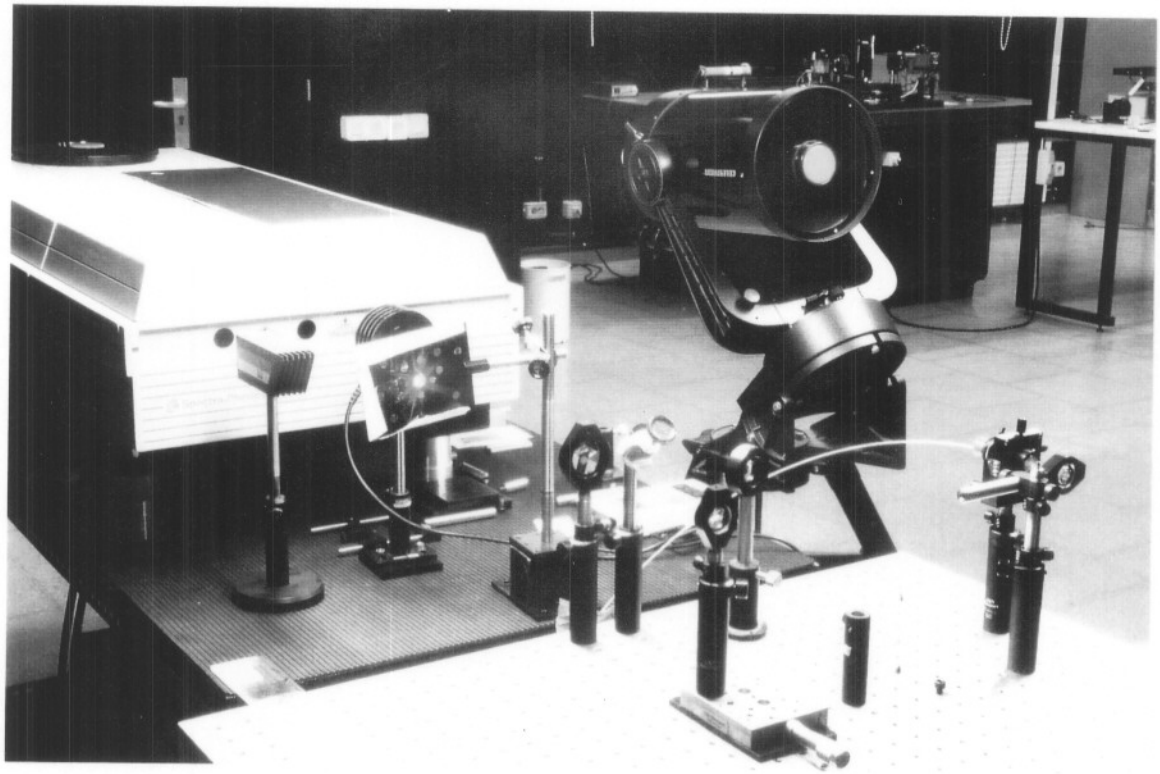

Fig. 29 System test experiment using the telescope.

4.4 Build-up correction

In the reported experiments a difficult point was time-range calibration of the system. If the build-up correction is not included, Advanced Sync signal jitter is translated into a maximum error of *52 m (7 samples)*. This error cannot be corrected by accurate calibration since it is not a systematic error.

To solve the problem, the build-up output was used and eq.(3) (Sect.1.2.2) was tested in the control program (Sect.3.3.2) with unsucessful results. Range correction still failed to be accurate enough. Finally, a decision was made in favour of programming a fixed value for T_{adv} and make a linear regression that took into account the build-up time $T_{b.}$ The linear regression is expressed as follows:

$$T_{ADV-SYNC} = 671.5 + 349.5\frac{V_b}{10} \quad [ns] \tag{20}$$

where V_b is the build-up voltage measured at the output of the build-up driver of Fig.1. Note that the correction slope *($\approx$35 ns/V)* is larger than the manufacturer's specification given by eq.(3).